Targeting SLC7A11-mediated cysteine metabolism for the treatment of trastuzumab resistant HER2 positive breast cancer

Yijia Hua[1,2,#], Ningjun Duan[1,#,*], Chunxiao Sun[1], Fan Yang[1], Min Tian[1], Yanting Sun[1], Shuhan Zhao[3], Jue Gong[1], Qian Liu[1], Xiang Huang[1], Yan Liang[1], Ziyi Fu[1], Wei Li[1], Yongmei Yin[1,2,4,*]

1. Department of Oncology, The First Affiliated Hospital of Nanjing Medical University, Nanjing, China

2. Gusu School, Suzhou Municipal Hospital, The Affiliated Suzhou Hospital of Nanjing Medical University, Suzhou, China

3. Department of General Surgery, The First Affiliated Hospital of Nanjing Medical University, Nanjing, China

4. Jiangsu Key Lab of Cancer Biomarkers, Prevention and Treatment, Collaborative Innovation Center for Personalized Cancer Medicine, Nanjing Medical University, Nanjing, China

# These authors contributed equally to this work.

*__Correspondence to__: Yongmei Yin, Email: ymyin@njmu.edu.cn

Ningjun Duan, Email: ningjun_official@outlook.com

Keywords:

HER2 positive breast cancer, trastuzumab primary resistance, cysteine metabolism, epigenetic modifications.

Abbreviations:

4-HNE, 4-hydroxynonenal; 5-mC, 5-methylcytosine; ADCC, antibody dependent cellular cytotoxicity; DAMPs, damage-associated molecular patterns; DMR, differentially methylated regions; GABA, 4-aminobutyric acid; GSH, glutathione; GSR, glutathione reductase; GSS, glutathione synthetase; GSSG, glutathione disulfide; HER2, human epidermal growth factor receptor 2; MDA, Malondialdehyde; pCR, pathological complete response; PUFAs, polyunsaturated fatty acids; PUMA, p53

upregulated modulator of apoptosis; sgRNA, small guide RNA; siRNA, short interfering RNA; SNP, single nucleotide polymorphism; SNV, single nucleotide variation; TCA, tricarboxylic acid; TME, tumor microenvironment; TNBC, triple negative breast cancer; WGBS, whole-genome bisulfite sequencing.

Author Contributions

Y.M.Y. and N.J.D. conceived the project. Y.J.H., N.J.D., C.X.S., F.Y., Y.T.S., S.H.Z., Y.L. and J.G. performed the experiments. M.T. and Q.L. helped collect clinical samples. Y.J.H. and N.J.D. conducted data analysis and wrote the manuscript. N.J.D., X.H., Z.Y.F., W.L. and Y.M.Y. supervised the study. All authors reviewed the manuscript.

Acknowledgements

We would like to thank the Core Facility of the First Affiliated Hospital of Nanjing Medical University for its help in the detection of experimental samples.

Funding

This project was supported by National Natural Science Foundation of China (81972484 and 82272667 to Yongmei Yin; 82203488 to Ningjun Duan), High-level Innovation Team of Nanjing Medical University Program (JX102GSP201727), The Collaborative Innovation Center for Tumor Individualization Program (JX21817902/008) and Beijing Xisike Clinical Oncology Research Foundation (Y-2019AZZD-00680).

Conflict of interest statement

The authors declare that there is no conflict of interest.

Data Availability

Further information and requests for resources could be directed to corresponding authors.

Abstract

Trastuzumab resistance remains a challenge for HER2 positive breast cancer treatment. Targeting metabolic reprogramming would provide novel insights for therapeutic strategies. Here, we integrated metabolomics, transcriptomics and epigenomics data of trastuzumab sensitive and primary resistant HER2 positive breast cancer to identify metabolic alterations. Aberrant cysteine metabolism was discovered in trastuzumab primary resistant breast cancer at both circulating and intracellular levels. The inhibition of SLC7A11 and cysteine starvation could synergize with trastuzumab to induce ferroptosis. Mechanistically, increased H3K4me3 and decreased DNA methylation enhanced SLC7A11 transcription and cystine uptake in trastuzumab resistant breast cancer. The regulation of epigenetic modifications modulated cysteine metabolism and ferroptosis sensitivity. These results revealed an innovative approach for overcoming trastuzumab resistance by targeting specific amino acid metabolism.

Introduction

Accounting for 15%-20% of all breast cancer cases, human epidermal growth factor receptor 2 (HER2) positive breast cancer has posed great threats to the health of women worldwide(1, 2). The overexpression of HER2 results in aberrant breast cancer cell proliferation, invasion, and progression(3). As a monoclonal antibody targeting HER2, trastuzumab has been recognized as the foundational medication in HER2 positive breast cancer treatment and provided remarkable clinical benefits for numerous patients(4). Around 50% HER2 positive breast cancer patients would experience trastuzumab resistance and disease progression during or after treatment settings(5). Current theories maintained that trastuzumab resistance mainly resulted from HER2 mutation(6), antigenic epitope variation(7), compensatory pathway activation(8) and tumor heterogeneity(9). However, there still lacks a comprehensive theory to thoroughly explain the mechanisms behind trastuzumab resistance, and exploring effective targets to overcome resistance remains a major topic in the field of

breast cancer research(3).

Metabolic reprogramming has been acknowledged as one crucial cancer hallmark(10). Traced back to the first study carried out by Otto Warburg, decades of studies have indicated that glycolysis, tricarboxylic acid (TCA) cycle, lipid metabolism, amino acid metabolism, as well as other processes collectively modulate the development and function of cancer cells and tumor microenvironment (TME) components(11-13). Several studies have revealed that different breast cancer subtypes featured diverse metabolic patterns(14, 15). Targeting specific enzymes or modulating nutrients uptake might normalize the TME and enhance breast cancer treatment efficacy(16, 17). Yet previous studies often focused on the overall metabolic subtypes of breast cancer, with little attention given to abnormal metabolic changes and underlying genomic alterations induced by specific drug resistance. This might lead to a poor understanding on the tumor heterogeneity in drug resistant breast cancer cells.

Epigenetic modifications play crucial roles in all stages of cancer development and contribute to cancer cell survival selection(18). Alterations in chromatin structure, DNA methylation and histone modifications provide tumor growth advantage and increase phenotypic variability(19). During the formation of drug resistance, epigenetic dysregulation modulates key genes transcription associated with treatment tolerance, leading to resistant clonal derivatives and disease progression(20). Previous studies suggested that COMPASS complex inactivation suppressed tumor suppressor genes transcription and accelerated breast cancer tumorigenesis(21). Aberrant DNA methylation resulted in abnormal oncogenic signaling activation and drug resistance acquisition(22). Targeting epigenetic reprogramming might provide novel treatment options for overcoming breast cancer drug resistance.

By integrating metabolomic, transcriptomic and epigenomic data, we identified metabolic alternations, especially cysteine-associated pathways, accompanied with the epigenetic changes during the development of primary trastuzumab resistance of HER2 positive breast cancer (**Figure 1A**). Based on these discoveries, targeting certain metabolism-related protein, epigenetic modification or nutrition could all be possible ways to overcome trastuzumab resistance. In all, our study provided novel

insights and potential solutions on primary trastuzumab resistance of HER2 positive breast cancer.

Methods

Patient cohort and blood samples collection

One breast cancer patient cohort from Jiangsu Province Hospital was embedded in this study, which consists of 26 primary trastuzumab resistant patients defined as disease recurrence during or after (≤ 12 months) trastuzumab adjuvant treatment and 26 trastuzumab sensitive patients that benefited from trastuzumab adjuvant treatment more than 12 months(23).

All blood samples were collected before the first trastuzumab treatment cycle. Samples collection was under the approval of the Ethics Committee and Institutional Review Board of Jiangsu Province Hospital. Each patient provided written informed consent for sample and data use.

Cell culture

Human breast cancer cell lines JIMT1, SKBR3 and human breast epithelial cell line MCF10A were obtained from American Type Culture Collection (ATCC). JIMT1 and SKBR3 cell lines were cultured in high-glucose Dulbecco's modified eagle medium (DMEM; Gibco, 11965092) with 10% fetal bovine serum (FBS; Gibco, 16140071) and 1% penicillin streptomycin (Gibco, 15140122) at 37□ with 5% CO_2. MCF10A was cultured in mammary epithelial cell growth medium (MEGM) supplemented with bovine pituitary extract, human epidermal growth factor, hydrocortisone, gentamicin sulfate-amphotericin, and insulin (Lonza, CC-3150) with 100 ng/ml cholera toxin (Sigma, C8052) at 37□ with 5% CO_2. Cell culture with cysteine starvation was performed by cystine/cysteine-deficient DMEM (BIOTREE) and 1% penicillin streptomycin at 37℃ with 5% CO_2.

DNA constructs, plasmids, and transfection

Short interfering RNA (siRNA) targeting ASH2L, SLC7A11 and GPX4 were presented in Supplementary Table S1. The design of small guide RNA (sgRNA) was

based on the relevant methylated region and conducted via the online tool CRISPick(24, 25). Sequences of sgRNA were indicated in Supplementary Table S2. dCas9-DNMT3A was obtained from Addgene (#100090)(26).

Transfection was conducted by using Lipofectamine 3000 (Invitrogen, L3000015) according to the manufacturer's protocol. In brief, cells were cultured in a six-well plate at 70%-90% confluency. For RNA interference, 2500 ng siRNA and 3.75 μl Lipofectamine 3000 reagents were mixed and then added in each well. For CRISPR-based epigenetic editing, dCas9-DNMT3A plasmid and sgRNA were first mixed in 1:2 ratio, then mixed with 3.75 μl Lipofectamine 3000 reagent and 5 μl P3000 reagent in each well.

Protein extraction and Western blots

Cells were collected and then lysed in SDS lysis buffer with phenylmethyl-sulfonyl fluoride (PMSF; Servicebio, G2008) and phosphatase Inhibitor cocktail (Servicebio, G2007) on ice. Proteins were seprated in SDS-PAGE and transferred to PVDF membranes (Millipore, IPVH00010). After blocked, membranes were incubated with specific primary and secondary antibodies, and then visualized with imaging system and ECL chemiluminescence kit (Vazyme, E422-01). Primary antibodies included SLC7A11 (CST, 12691S), GPX4 (CST, 52455S), glutathione synthetase (Abcam, ab124811), glutathione reductase (Abcam, ab124995), ASH2L (CST, 5019T), H3K4me3 (Abcam, ab213224), GAPDH (proteintech, HRP-60004), and H3 (Abcam, ab1791). The secondary antibody was horseradish peroxidase (HRP) conjugated goat anti-rabbit IgG(H+L) (ImmunoWay, RS0002).

GSH/GSSG ratio assay

GSH/GSSG ratio was measured with a GSH and GSSG assay kit (Beyotime, S0053). Cells were lysed with protein removing reagent solution and several freeze-thaw cycles. After centrifuged, supernatants were collected and incubated with DTNB and NADPH.

The absorbance at 412 nm was detected to measure the GSH/GSSG ratio with standard curve.

C11 BODIPY (581/591) assay

Cells were collected and incubated with 5 μM C11 BODIPY (581/591) (invitrogen, D3861) for 30 minutes at 37 □. The oxidated and reduced state were detected by flow cytometry, with excitation and emission wavelength at 488/510 and 581/591 nm, respectively.

DCFH-DA assay

Cells were collected and incubated with 10 μM DCFH-DA (MCE, HY-D0940) for 30 minutes at 37 □. The oxidated state was detected with laser excitation wavelength at 488nm.

Cystine uptake assay

The cystine uptake ability was measured by using cystine uptake assay kit (DOJINDO, UP05). Cells were incubated with cystine analog solution and fluorescent probe. The fluorescence intensity was measured with excitation and emission wavelength at 490 and 535 nm.

Quantification of intracellular cysteine

The concentration of intracellular cysteine was detected by using a cysteine quantification kit (Solarbio, BC0185). Cells were lysed and incubated with solution containing phosphotungstic acid. The absorbance at 600nm was detected to measure intracellular cysteine levels.

ChIP

Chromatin extraction and the following immune precipitation were performed with chromatin extraction kit (Abcam, ab117152) and ChIP kit (Abcam, ab117138) according to manufacturer's protocols. Cells were harvested and treated with 1% formaldehyde first, then sonication was applied on cross-linked chromatin to generate 200-1000 bp fragments. Chromatin fractions enriched with certain histone modifications were captured by antibodies (H3K27me3 (CST, C36B11), H3K4me3 (Abcam, ab213224) and IgG) and released by protease digestion.

RT-qPCR was applied to quantify the enrichment of specific type of histone modification at certain chromatin regions with ChamQ SYBR qPCR Master Mix (Vazyme, Q311). While VAHTS® Universal DNA Library Prep Kit for Illumina (Vazyme, ND607) and Illumina Novaseq 6000 platform were applied for sequencing

library preparation and the following sequencing. All primers used for ChIP-qPCR were presented in Supplementary Table S3.

MeDIP

Methylated DNA immune precipitation was performed with MeDIP kit (Abcam, ab117135) according to manufacturer's protocols followed by chromatin extraction as ChIP protocol. After cross-linking and sonication, methylated chromatin fractions were enriched by anti-5-Methylcytosine (5-mC) antibody (CST, 28692). RT-qPCR was applied to quantify the enrichment of 5-mC at certain chromatin regions. All primers used for MeDIP-qPCR were presented in Supplementary Table S3.

Dot Blots

Total genomic DNA was extracted by using nucleic DNA isolation kit (Vazyme, DC112). Denaturized DNA was spotted on a nitrocellulose membrane, and blocked with 5% skim milk in TBST (20mM Tris, 150mM NaCl, and 0.1% Tween-20). Anti-5-mC primary antibody and HRP-conjugated secondary antibody together with ECL chemiluminescence kit were applied for total methylated cytosine visualization.

Mice xenograft model construction

Six-week-old female BALB/c nude mice were obtained from Beijing Vital River Laboratory Animal Technology, housed in a 12-hour light-dark lighting condition with 20-22 ℃ temperature and 60 ± 10% humidity. The animal diet and drinking water followed the national standard for experimental animal feed. The diet underwent Cobalt-60 irradiation sterilization and the drinking water followed purification and sterilization.

All animal experiments were conducted according to the review and approval of Institutional Animal Care and Use Committee in Nanjing Medical University (IACUC-2204057). 3×10^6 JIMT1 cells were injected subcutaneously into the mammary fat pad region to generate xenograft models.

The mice were divided into 6 groups: (1) DMSO treatment; (2) trastuzumab (Roche) treatment (10mg/kg, injected intraperitoneally twice a week); (3) erastin (HY-15763) treatment (40mg/kg, injected intraperitoneally every other day); (4) cysteine

starvation; (5) trastuzumab treatment plus cysteine starvation; (6) trastuzumab plus erastin treatment. Cysteine starvation was performed by utilizing cystine/cysteine deficient diet (Xietong Bio). Treatment was initiated when tumor volume reached $50mm^3$. Tumor sizes and mice weight were measured three times a week. Tumor volumes were calculated as $0.5 \times L \times W^2$ (L: the longest dimension, W: the perpendicular dimension). The tumor growth was compared by paired individual fold change of tumor volumes.

Tumor and spleen cell composition analysis

Tumor samples were digested in serum-free RPMI with 10mg/ml collagenase I (Sigma, C0130) and 1mg/mg DNase I (Roche, 10104159001) for 30-60 minutes at 37 □. Spleen samples were gently crushed. Both of them were filtered in 70μm strainers, followed by red blood cell removement with RBC lysis buffer (eBioscience, 00-4333-57), and then resuspended in flow cytometry staining buffer. Fc receptor was blocked with mouse FcR blocking reagent (Miltenyi, 130-092-575).

Fluorescent antibodies including CD45 (clone 30-F11, eBioscience, 48-0451-82), CD3 (clone 145-2C11, BioLegend, 100353), CD49b (clone DX5, BioLegend, 108907), CD11b (clone M1/70, eBioscience, 56-0112-82), CD27 (clone LG.3A10, BioLegend, 124216), CD335 (NKp46) (clone 29A1.4, eBioscience, 17-3351-82) and granzyme B (clone NGZB, eBioscience, 11-8898-82) together with fixable viability dye (eBioscience, 65-0865-14) were chosen for cell staining. CytoFLEX (Beckamn Coulter) and FlowJo software were applied for fluorescence measurement and analysis.

Immunohistochemical staining

After formalin fixation and paraffin embedding, tissue sections were cut and mounted on slides followed by deparaffinizing, rehydrating and antigen retrieval. Samples were then stained with antibodies including SLC7A11 (Abcam, ab307601), GPX4 (Abcam, ab125066), 4-Hydroxynonenal (4-HNE) (Abcam, ab48506), Malondialdehyde (MDA) (Abcam, ab243066), and caspase-3 (Abcam, ab32150).

Differential transcriptome analyses

The human hg38 genome was utilized for RNA sequencing reads alignment.

Differential expression analyses were measured by the DESeq2 package in R. Significant differential expression was defined with a threshold of P adj ≤ 0.05 and |log2 fold change| ≥ 0.5.

Differential metabolome analyses

Metabolomics data was analyzed by the MetaboAnalystR package in R(27). Pathway enrichment analyses was performed according to KEGG databases. Significant difference was defined with a threshold of P adj ≤ 0.05 and |log2 fold change| ≥ 0.5.

Differential epigenome analyses

Sequencing reads of ChIP and whole-genome bisulfite sequencing (WGBS) were aligned to the human hg38 genome. Differential methylation analyses was performed by deepTools (version 3.5.5)(28). Differentially methylated regions (DMR) were identified by Bismark (version 0.24.2)(29). Significant difference was defined with a threshold of P adj ≤ 0.05 and |log2 fold change| ≥ 0.5.

Genomics analyses

The human hg38 genome was utilized to align WGS sequencing reads. Germline single nucleotide polymorphisms (SNP) and Indels were identified by GATK (v 4.5.0.0). The annotation of germline mutations was obtained by utilizing ANNOVAR.

Statistical analyses

All statistical analyses were performed by utilizing GraphPad Prism (version 10.1.2) and R (version 4.3.3). All data were represented as the mean ± standard error (SE) or the mean ± SEM from a minimum of three independent experiments. Two-tailed Student's t-test was applied to determine statistical in comparisons between two groups and ANOVA test in multiple groups. The threshold for statistical significance is P <0.05, and was marked as * $P < 0.05$, ** $P < 0.01$, *** $P < 0.001$.

Results

Different amino acids metabolic patterns between trastuzumab sensitive and primary resistant HER2 positive breast cancer patients

To investigate metabolic patterns of HER2 positive breast cancer patients with different trastuzumab response, we obtained and analyzed the plasma metabolites data

of both trastuzumab sensitive and primary resistant patients (26/26) with good interclass correlations (**Figure S1A-C**). Of them, 203 metabolites (130 upregulated and 73 downregulated in primary resistant groups) were identified with different abundances among two patient groups (**Figure 1B and S1D**). KEGG-based pathway analyses suggested the major enrichment in amino acids metabolism. For instance, glycine, serine and threonine metabolism, valine, leucine and isoleucine biosynthesis, as well as cysteine and methionine metabolism were reduced in primary resistant patients; while arginine, proline, alanine, aspartate and glutamate metabolism were enhanced (**Figure 1C and 1D**).

By comparing the abundance of 20 common protein-construction amino acids, we realized that cystine and aspartate were higher while valine, lysine and leucine were lower in primary resistant groups. However, glutamate kept stable in both groups (**Figure 1E and 1F**). Non-protein amino acids also displayed difference among these two groups. 2-aminoisobutyric acid and 4-aminobutyric acid (GABA) were lower in resistant groups, while citrulline, kynurenine, ornithine and taurine levels were similar (**Figure S1E**).

We then analyzed transcriptomic data of pre-treatment breast cancer tumors in I-SPY2 trial(30) to further explore metabolic gene alterations, in which HER2 positive breast cancer patients received trastuzumab plus paclitaxel, trastuzumab combined with pertuzumab and paclitaxel or T-DM1 plus paclitaxel during neoadjuvant settings. By comparing patients with different responses to neoadjuvant trastuzumab-based regimens (pathological complete response [pCR] and non-pCR), we found 1542 genes upregulated and 1350 genes downregulated in non-pCR groups (**Figure S1F and 1G**). Based on KEGG datasets, amino acids metabolism was found dysregulated in patients with poor responses to trastuzumab, including aberrant lysine degradation, cysteine and methionine metabolism, beta-alanine metabolism and histidine metabolism (**Figure 1H**).

As cystine was one of the most significant amino acids in both metabolomic and transcriptomic analyses, we investigated relations between cystine/cysteine metabolic key genes and trastuzumab treatment outcomes. Patients with non-pCR featured

higher expression of SLC7A11, while no differences were found in GPX4, GSS and GSR expression (**Figure 1I**), indicating SLC7A11 might become a potential target for trastuzumab primary resistant patients.

In general, trastuzumab primary resistant HER2 positive breast cancer patients featured distinct amino acids metabolic patterns, especially increased plasma cystine levels and higher expression of SLC7A11.

Distinct cysteine metabolism in trastuzumab primary resistant HER2 positive breast cancer

To comprehensively compare the metabolic heterogeneity between trastuzumab sensitive and primary resistant HER2 positive breast cancer, we obtained and analyzed both metabolomic and transcriptomic data of trastuzumab sensitive SKBR3 and trastuzumab resistant JIMT1 cell lines.

Significant differences were observed in metabolic data with good quality (**Figure S2A and S2B**). Specifically, 181 upregulated and 235 downregulated hydrophilic metabolites accompany 546 upregulated and 412 downregulated lipophilic metabolites were found in JIMT1 cells compared to SKBR3 cells (**Figure 2A and S2C**). For hydrophilic metabolites, enrichment analyses revealed that glycine, serine and threonine metabolism were upregulated in JIMT1, while cysteine and methionine metabolism were downregulated (**Figure 2B and 2C**). Enrichment analyses based on lipophilic metabolites showed that linoleic acid metabolism, fatty transportation and glycerophospholipid catabolism were upregulated in JIMT1, but glycerolipid metabolism, phospholipid biosynthesis and retinoid metabolism downregulated (**Figure S3A and S3B**).

Differential gene expression could also be uncovered from transcriptomic data. 4235 downregulated genes and 4923 upregulated genes were identified in the comparison between JIMT1 and SKBR3 cells (**Figure S4A**). Based on KEGG datasets, activities of cysteine and glutathione metabolism pathways were found dysregulated in JIMT1 cells (**Figure 2D**). More importantly, the joint pathway analyses combining metabolomic and transcriptomic data indicated that JIMT1 featured aberrant

glutathione metabolism (**Figure 2E**).

The extracellular cystine is mainly imported by SLC7All for subsequent protein synthesis, glutathione (GSH) production and oxidative catabolism (**Figure 2F**). Both transcriptomic and protein evidence revealed the upregulation of SLC7A11 and glutathione synthetase (GSS) as well as the downregulation of GPX4 and glutathione reductase (GSR) in JIMT1 cells (**Figure S4B and 2G**), together with the characteristics that JIMT1 cells showed higher cysteine uptake ability and cytoplasmic cysteine level but lower glutathione/glutathione disulfide (GSH/GSSG) ratio than SKBR3 cells (**Figure 2H-J**), indicating the probably increased transsulfuration activity and decreased γ-glutamyl-peptides synthesis activity in JIMT1 cells (**Figure S4C**). These results suggested that HER2 positive breast cancer with primary trastuzumab resistance might prefer to consume more cystine and feature intracellular cysteine metabolic reprogramming, showing high consistency with metabolic characteristics of relevant breast cancer patients and may associate with trastuzumab treatment response.

Stimulate ferroptosis sensitivity of trastuzumab primary resistant HER2 positive breast cancer

Since cysteine metabolism plays key role in maintaining cellular oxidative-reductive balance, disruption of which may turn breast cancer cells into a more sensitive state to oxidative damage, including ferroptosis(31, 32). We first downregulated the expression of SLC7A11 and GPX4 in JIMT1 by siRNAs, and the lipid peroxidation of ferroptosis was found increased by measuring BODIPY-C11 (**Figure 3A and 3B**). Similar results were also detected in SKBR3(**Figure S5A and S5B**). We then detected the sensitivity of JIMT1 and SKBR3 to SLC7A11 inhibitor (erastin) and GPX4 inhibitor (RSL3) and found JIMT1 was more sensitive to these two inhibitors (**Figure S5C and S5D**). The deprivation of cysteine could suppress the growth of both JIMT1 and SKBR3, but JIMT1 showed more tolerance to this nutrition starvation (**Figure S5E**).

12 hours treatment of SLC7A11 inhibitor (erastin), GPX4 inhibitor (RSL3) and even

cysteine starvation were all able to induce ferroptosis in both JIMT1 and SKBR3 cells (**Figure 3C and 3D**). However, JIMT1 cells indicated more rapidly accumulation of lipid peroxidation under the treatment of erastin, which could be detected by both increased BODIPY-C11 and DCFH-DA (**Figure 3E and 3F**). Compared with SKBR3, JIMT1 cells were also more sensitive to RSL3 but more durable to cysteine starvation (**Figure 3G and 3H**), which might be explained by its stronger transsulfuration activities and decreased γ-glutamyl-peptides synthesis (**Figure S5F**). The utilization of ferroptosis inhibitor Fer-1 could suppress the lipid peroxidation resulted from erastin, RSL3 and cysteine starvation in both JIMT1 and SKBR3, which also indicated the role of cysteine metabolism in modulating HER2 positive breast cancer ferroptosis (**Figure S5G and S5H**).

To understand whether trastuzumab would modulate the ferroptosis sensitivity, we treated JIMT1 cells with trastuzumab for different durations. We found that with a prolonged exposure of trastuzumab for 72 hours, the total amount of SLC7A11 in JIMT1 was decreased (**Figure 3I**). Correspondingly, cystine uptake ability was suppressed after trastuzumab treatment for 48 and 72 hours (**Figure 3J**). In addition, cells underwent trastuzumab treatment combining with erastin or cysteine starvation could demonstrate stronger lipid peroxidation and enhanced ferroptosis (**Figure 3K**).

Restraining cysteine metabolism inhibited tumor growth in vivo

To further investigate the effects of SLC7A11 inhibition or cysteine limitation on trastuzumab primary resistant HER2 positive breast cancer, JIMT1 xenograft mouse models were generated and then treated with different strategies including DMSO, trastuzumab, erastin, cysteine starvation, trastuzumab plus erastin, and trastuzumab plus cysteine starvation (**Figure 4A**).

Of them, trastuzumab plus erastin and trastuzumab plus cysteine starvation could effectively inhibit tumor growth, while cysteine starvation and erastin monotherapy only showed limited effects on tumor progression, demonstrating the better treatment responses of combination strategy (**Figure 4B, 4C and S6A**). In addition, almost no weight differences were observed among all groups during treatment, partially

indicating the safety of such cysteine limitation treatment (**Figure 4D**).

The immune cell compositions in tumor and spleen of each group were measured to analyze the immune response induced by different treatment strategies (**Figure S6B and S6C**). The infiltration of NK cells (CD3-CD45+CD49b+) in tumors was increased only upon the combination of cysteine deprivation and trastuzumab (**Figure 4E**). Nearly no differences were found in tumor infiltrating NK cell activation (NKp46), toxic function (Granzyme B) and maturation status (CD11b, CD27) among all these groups (**Figure 4F-H**). While similar results were also observed in spleen NK cells (**Figure S6D-G**).

These results suggested a better effect of cysteine starvation than erastin in NK cell recruitment and activation, resulting a more powerful synergy with trastuzumab to increase the abundance of tumor infiltrating NK cells and show better inhibition of trastuzumab primary resistant breast cancer. As the anti-tumor effects of trastuzumab mainly relies on antibody dependent cellular cytotoxicity (ADCC) effects mediated by NK cells(33), this combination therapy might provide more effective approaches for HER2 positive breast cancer treatment.

We then analyzed the biomarkers of cysteine metabolism and cell death pathways in tumor samples of different treatment groups (**Figure 4I)**. Erastin and cysteine deprivation monotherapy, or combined with trastuzumab, could upregulate SLC7A11 and GPX4 expression, as well as the abundance of MDA and 4-HNE. Ferroptosis might increase endoplasmic reticulum stress and activate p53 upregulated modulator of apoptosis (PUMA)(34). The combination of trastuzumab and erastin or trastuzumab and cysteine starvation might also modify apoptosis sensitivity. Apoptosis biomarker caspase-3 was found increasing in these synergic treatment groups (**Figure S6H**). These results suggested that targeting cysteine metabolism could induce ferroptosis in trastuzumab primary resistant HER2 positive breast cancer and might have a synergic effect with trastuzumab to inhibit breast cancer progression.

Aberrant promoter H3K4me3 regulates SLC7A11 gene expression and cysteine

metabolism

Abnormal changes of histone modification play critical roles in tumor progression including drug resistance(35). Of them, altered methylations on promoter histone H3K4 and H3K27 show most important effects on gene expression(36).

By comparing the ChIP-seq data, we detected 3934 and 3925 H3K4me3 peaks were enriched in JIMT1 and SKBR3 respectively. These altered peaks primarily located among the promoter regions of genes (**Figure 5A and S7A**), which have close relationships with biological processes such as nucleic acid transcription, protein modification, mRNA processing and ribosome processing (**Figure S8A**)

We also confirmed that 7048 and 7001 H3K27me3 peaks were enriched in JIMT1 and SKBR3 respectively, mainly enriching at not only promoter regions but also distal intergenic regions, and exons (**Figure 5B and S7B**) of genes that involve in cell-cell adhesions, axon guidance, postsynaptic transmission, and neuron differentiation (**Figure S8B**).

Particularly, we uncovered the enrichment of H3K4me3 at the promoter regions of key cysteine transporter gene SLC7A11 in JIMT1 cells compared with SKBR3 cells while H3K27me3 signals were stable (**Figure 5C**), showing the consistency with its high expression in JIMT1 cells.

By inhibiting the expression of ASH2L, one crucial subunit of COMPASS complex(37), we downregulated not only the overall H3K4me3 level but also the signal at SLC7A11 promoter in JIMT1 cells, and successfully decreased the expression of SLC7A11 (**Figure 5D-F**). Meanwhile, diminished downstream cysteine uptake leaded to increased lipid peroxidation, the key symbol of ferroptosis (**Figure 5G and 5H**).

These results suggested that H3K4me3 may play a more important role in modulating SLC7A11 transcription and cysteine metabolism in JIMT1 than H3K27me3. Targeting H3K4me3 could regulate SLC7A11 expression, enhancing lipid peroxidation and inducing ferroptosis.

DNA methylation modifies SLC7A11 transcription and cysteine metabolism

Besides histone modification, DNA methylation is another crucial epigenetic modification to regulate genomic imprinting, modify transposable elements and modulate transcription, even in tumor progression(38).

In general, JIMT1 cells featured a lower abundance of total 5-mC than SKBR3 cells (**Figure S9A**). By investigating DNA methylation landscape with WGBS, we identified 329419 CG-DMRs enriched in JIMT1 and 84634 CG-DMRs enriched in SKBR3 (**Figure 6A and S9B**). Among non-CG DMRs (CHG, CHH; in which H denotes A, C or T), 1604 CHG-DMRs and 3727 CHH-DMRs were upregulated in JIMT1, while 2187 CHG-DMRs and 5158 CHH-DMRs were upregulated in SKBR3 (**Figure S9B**).

Across whole genome, CG-DMRs mainly enriched in intron, intergenic regions, and exons (**Figure S9C**). Differentially methylated genes were related to several biological processes, such as neurotransmitter biosynthesis, postsynaptic transmission, cytoplasmic translation, and ribosomal activities (**Figure S10A and S10B**).

SLC7A11 is located at chromosome 4q28.3 and we found that, in comparison with SKBR3, the CpG methylation at SLC7A11 promoter region was decreased in JIMT1 (**Figure 6B**). To further verify the influence of altered promoter GC-DMR on SLC7A11 gene transcription, CRISPR/Cas9-based genomic editing tool dCas9-DNMT3A together with SLC7A11 specific promoter-targeting sgRNA sets were utilized to successfully increase the 5-mC level at SLC7A11 promoter regions (**Figure 6C**) in JIMT1 cells, which is confirmed by MeDIP-qPCR (**Figure 6D**). As a result, the expression of SLC7A11 and cysteine uptake were reduced (**Figure 6E and 6F**), and the following cellular lipid peroxidation and ferroptosis were stimulated in JIMT1 cells (**Figure 6G**).

These results revealed that increased DNA methylation at SLC7A11 promoter regions in JIMT1 might contribute to SLC7A11 overexpression. Precise modulation of 5-mC could suppress cysteine uptake and result in ferroptosis, which might provide novel methods to overcome trastuzumab resistance.

Discussion

Metabolic heterogeneity has been widely accepted as important characteristics in many cancer types, which are closely associated with cancer progression, distant metastasis, and even drug resistance(39, 40), while targeting dysregulated metabolism could also be novel therapeutic strategies(41).

By comparing the metabolomic data of cell lines and blood samples from patients, we realized that widespread metabolic reprogramming particular the alternation of cysteine metabolism was an important feature of primary trastuzumab resistance, extending our understanding of anti-tumor drug resistance (**Figure 7**).

Cysteine is a crucial non-essential amino acid and mainly obtained from dietary, protein catabolism and methionine transsulfuration(42). Due to oxidative extracellular environment, cystine, instead of cysteine, is normally intake by the major transporter SLC7A11 (also known as xCT)(43), which also has important roles in protein synthesis, posttranslational modifications, and redox balance maintenance(42, 44).

Meanwhile, biosynthesis of GSH by GSS is one important outlet of cellular cysteine, which helps maintaining oxidation-reduction balance and protecting membrane from oxidative damage including ferroptosis with GPX4 and GSR(45, 46). The downregulation of both GPX4 and GSR and the upregulation of GSS, together with the higher intake of cysteine mediated by raised SLC7A11, could stimulate GSH consumption and GSSG accumulation in JIMT1 cells, resulting in a weaker reductive cytoplasmic environment and higher sensitivity to oxidative damage, including ferroptosis.

As an important rate-limiting metabolite of the GSH biosynthesis, cysteine modulates ferroptosis through the cyst(e)ine/GSH/GPX4 axis(47). SLC7A11 inhibition, cysteine deprivation or targeting GPX4 have been reported to effectively enhance lipid peroxidation and induce ferroptosis in several cancer types(48-51). In our study, JIMT1 was much more sensitive to SLC7A11 and GPX4 inhibition, but tolerable to cysteine starvation, and this might result from increased methionine transsulfuration activity and γ-glutamyl-peptides synthesis, which compensated the deficiency of extracellular cysteine(52, 53). Whether similar effects could be observed on GSS or

GSR also need to be studied.

The inhibition of HER2 could result in impaired redox homeostasis and increased ROS(54). Tumor cells might adapt to this metabolic stress by activating antioxidant signaling pathways and acquire recurrence and dormancy(54, 55). Although JIMT1 is resistant to trastuzumab, the extended exposure of trastuzumab was found to decrease SLC7A11 expression. SLC7A11 overexpression and altered cysteine and glutathione metabolism might function as compensating ways for trastuzumab adaptation. The dual inhibition of cysteine metabolism and HER2 also enhanced ferroptosis both in vivo and in vitro. In a similar manner, the inhibition of glutamine metabolism and antioxidant transcription factor NRF2 could also suppress the proliferation of residual breast cancer after HER2 inhibition and restore intracellular GSH metabolism(54). These results indicated that re-establishing redox homeostasis and modulating antioxidant metabolism might provide novel treatment options for trastuzumab primary resistant HER2 positive breast cancer.

Besides amino acids metabolism, lipid metabolism, especially polyunsaturated fatty acids (PUFAs) and relevant phospholipid metabolism, which are also key drivers of ferroptosis(56), were identified dysregulated in both primary and acquired trastuzumab resistance of HER2 positive breast cancer(57), demonstrating the possibility that targeting PUFA metabolism to induce ferroptosis might provide novel treatment options for overcoming trastuzumab resistance.

Not limited to cancer cells, altered cellular metabolism and oxidation-reduction balance can also affect activities of immune cells within TME(58-60). For example, lipid peroxidation stress might impair NK functions and immune surveillance. Metabolites, such as L-kynurenine, might enhance ferroptosis in NK cells through aryl hydrocarbon receptor and mediate immunosuppressive TME in gastric cancer(61). Activation of NRF2 related antioxidant pathways could restore NK cell functions and trigger enhanced anti-tumor responses(62). And The deprivation of cysteine was reported to promote the metabolic reprogramming of TME and influence T cell immune responses(63). We observed that the combination of cysteine starvation and trastuzumab can increase tumor infiltrating NK cells but show limited effects on NK

cell development and toxic functions, relevant mechanisms still need to be discussed. In addition, metabolites, cytokines, damage-associated molecular patterns (DAMPs) and other immunomodulatory signals released from cancer cells that undergo ferroptosis could function on immune cells nearby, stimulating or suppressing anti-tumor immune responses(64, 65).

The emergence of drug resistance in cancers mainly depends on two scenarios: Darwinian selection and Lamarkian induction(66, 67). During the evolution of breast cancer, different subtypes of breast cancer might originate from different development status of mammary stem cells, bipotent progenitors and differentiated cells(68, 69). HER2 positive breast cancer was reported to transform from luminal progenitor and mature luminal cells(70-72). The tumorigenesis of trastuzumab primary resistant HER2 positive breast cancer might favor the Darwinian selection, as a small population of pre-existing trastuzumab tolerant cancer cells might be enriched upon treatment.

To investigate genetic and epigenetic issues stimulating the evolution of primary trastuzumab resistant and sensitive breast cancer, we compared genomic variation, histone modification and DNA methylation status among JIMT1, SKBR3 and MCF10A (normal mammary epithelial cell).

During carcinogenesis, missense mutations, splicing mutations and in frame deletions were the most frequent events and MUC3A, MUC6, OR8U1 and ZNF717 were most frequent mutated genes (**Figure S11A and S11B**). Meanwhile, single nucleotide polymorphism (SNP) was the major variation type and the substitution between cytosine and thymine was the most common signature (**Figure S12A-B and S13A-C**).

Compared with MCF10A, JIMT1 instead of SKBR3 featured distinct single nucleotide variation (SNV) at the exon region of SLC7A11 (gain at Chr4:138183261 and loss at Chr4: 138219340) (**Figure S14A-C**).

SNVs located in exons have been reported to modulate gene transcription and function. For example, SNVs in BRCA1 exons encoding RING and BRCT domains might disrupt BRCA1 expression and function, therefore increasing breast cancer

risks(73). While noncoding SNVs, such as rs9383590 located at ESR1 enhancer region, could interact with regulatory elements and activate oncogene transcription(74). The accumulation of SNVs was also associated with driver gene mutations and might promote breast cancer evolution in a cumulative manner(75). Whether different SNVs in SLC7A11 exon regions could contribute to SLC7A11 expression and breast cancer initiation still needs to be studied.

Epigenetic issues also demonstrated their impact on carcinogenesis. H3K4me3 instead of H3K27me3 peaks were shown more enrichment at SLC7A11 promoter regions in MCF10A cells (**Figure S15A and S15B**), while 5-mC levels at CpG islands among SLC7A11 promoter regions were also increased in MCF10A (**Figure S15C**), revealing the important proposal of histone modifications and DNA methylation on metabolic reprogramming during the evolution of HER2 positive breast cancer.

Although several studies have reported that SLC7A11 expression was modulated by NRF2, ATF4 and other transcription factors(43, 76, 77), it remains unclear whether its expression is subject to a broader genome-wide or histone-level regulation(78). The theory that epigenetic modifications contribute to specific transcription regulation, cancer cell development and metabolic reprogramming, to modulate treatment response and drug resistance, has been widely accepted and proved(79). Our study tried to explore the relationship between the altered cysteine metabolism signature and epigenetic modifications in trastuzumab resistant HER2 positive breast cancer. Elucidating epigenetic mechanisms would help better understand trastuzumab resistance formation and provide novel therapeutic opportunities.

Several studies have described the regulatory roles of histone modifications on oncogene transcription(79, 80). MLL mutations were identified among various cancers and widespread shortening H3K4me3 peaks at tumor suppressor genes might contribute to tumor initiation(81, 82) and H3K27me3 could modulate chemotherapy tolerance in triple negative breast cancer (TNBC)(83). Moreover, the combination of chemotherapy and H3K27me3 demethylation inhibitor could prevent the proliferation of persister cells(83). Targeting KDM6A could inhibit JIMT1 tumor growth via decreasing tRNA transcription(84). As we confirmed, reducing H3K4me3 can

decrease ASH2L, SLC7A11 expression and cystine uptake, leading to enhanced lipid peroxidation and ferroptosis, modulating histone modification can be a promising strategy in cancer treatment.

Compared with normal tissues, almost all cancers feature abnormal DNA hypomethylation and local hypermethylation at specific CpG islands(81, 85). Dysregulated DNA methylation contributes to breast cancer tumorigenesis and drug resistance formation(86, 87). For instance, trastuzumab resistant HER2 positive breast cancer was found associated with downregulated TGFBI, CXCL2 and SLC38A1, which was silenced by DNA hypermethylation(88). Aberrant DNMT1, DNMT3A and DNMT3B expression were correlated with endocrine therapy resistance and predicted worsen pathologic status and prognosis(89). By utilizing CRISPR interference, we verified the effect of 5-mC at SLC7A11 promoter on gene expression and downstream cysteine metabolism. What's more, since increased H3K4me3 might interact with DNMT3A-DNMT3L(90), the crosstalk between histone modification and DNA methylation may have collaborative effects on cysteine metabolism in trastuzumab primary resistant breast cancer.

In conclusion, our study revealed that trastuzumab primary resistant HER2 positive breast cancer featured distinct cysteine metabolism, which was driven by altered H3K4me3 and DNA methylation. Targeting cysteine metabolism could provide novel treatment concepts for overcoming trastuzumab resistance.

Supplemental information

Figures S1-S15 and Tables S1-S3

References

1. Giaquinto AN, Sung H, Miller KD, et al. Breast Cancer Statistics, 2022. CA Cancer J Clin.

658 2022;72(6):524-41.

659 2. Harbeck N, Penault-Llorca F, Cortes J, et al. Breast cancer. Nat Rev Dis Primers.
660 2019;5(1):66.

661 3. Swain SM, Shastry M, Hamilton E. Targeting HER2-positive breast cancer: advances and
662 future directions. Nat Rev Drug Discov. 2023;22(2):101-26.

663 4. Marra A, Chandarlapaty S, Modi S. Management of patients with advanced-stage
664 HER2-positive breast cancer: current evidence and future perspectives. Nat Rev Clin Oncol.
665 2024;21(3):185-202.

666 5. Cossetti RJ, Tyldesley SK, Speers CH, et al. Comparison of breast cancer recurrence
667 and outcome patterns between patients treated from 1986 to 1992 and from 2004 to 2008. J
668 Clin Oncol. 2015;33(1):65-73.

669 6. Xu X, De Angelis C, Burke KA, et al. HER2 Reactivation through Acquisition of the HER2
670 L755S Mutation as a Mechanism of Acquired Resistance to HER2-targeted Therapy in
671 HER2(+) Breast Cancer. Clin Cancer Res. 2017;23(17):5123-34.

672 7. Arribas J, Baselga J, Pedersen K, et al. p95HER2 and breast cancer. Cancer Res.
673 2011;71(5):1515-9.

674 8. Baselga J, Cortes J, Im SA, et al. Biomarker analyses in CLEOPATRA: a phase III,
675 placebo-controlled study of pertuzumab in human epidermal growth factor receptor 2-positive,
676 first-line metastatic breast cancer. J Clin Oncol. 2014;32(33):3753-61.

677 9. Marchio C, Annaratone L, Marques A, et al. Evolving concepts in HER2 evaluation in
678 breast cancer: Heterogeneity, HER2-low carcinomas and beyond. Semin Cancer Biol.
679 2021;72:123-35.

680 10. Hanahan D. Hallmarks of Cancer: New Dimensions. Cancer Discov. 2022;12(1):31-46.

681 11. Martinez-Reyes I, Chandel NS. Cancer metabolism: looking forward. Nat Rev Cancer.
682 2021;21(10):669-80.

683 12. Vander Heiden MG, DeBerardinis RJ. Understanding the Intersections between
684 Metabolism and Cancer Biology. Cell. 2017;168(4):657-69.

685 13. Kao KC, Vilbois S, Tsai CH, et al. Metabolic communication in the tumour-immune
686 microenvironment. Nat Cell Biol. 2022;24(11):1574-83.

687 14. Gong Y, Ji P, Yang YS, et al. Metabolic-Pathway-Based Subtyping of Triple-Negative
688 Breast Cancer Reveals Potential Therapeutic Targets. Cell Metab. 2021;33(1):51-64 e9.

689 15. Xiao Y, Ma D, Yang YS, et al. Comprehensive metabolomics expands precision medicine
690 for triple-negative breast cancer. Cell Res. 2022;32(5):477-90.

691 16. Miller KD, O'Connor S, Pniewski KA, et al. Acetate acts as a metabolic immunomodulator
692 by bolstering T-cell effector function and potentiating antitumor immunity in breast cancer. Nat
693 Cancer. 2023;4(10):1491-507.

694 17. Xiao Y, Yu TJ, Xu Y, et al. Emerging therapies in cancer metabolism. Cell Metab.
695 2023;35(8):1283-303.

696 18. Timp W, Feinberg AP. Cancer as a dysregulated epigenome allowing cellular growth
697 advantage at the expense of the host. Nat Rev Cancer. 2013;13(7):497-510.

698 19. Feinberg AP, Koldobskiy MA, Gondor A. Epigenetic modulators, modifiers and mediators
699 in cancer aetiology and progression. Nat Rev Genet. 2016;17(5):284-99.

700 20. Brown R, Curry E, Magnani L, et al. Poised epigenetic states and acquired drug
701 resistance in cancer. Nat Rev Cancer. 2014;14(11):747-53.

702 21. Langille E, Al-Zahrani KN, Ma Z, et al. Loss of Epigenetic Regulation Disrupts Lineage
703 Integrity, Induces Aberrant Alveogenesis, and Promotes Breast Cancer. Cancer Discov.
704 2022;12(12):2930-53.
705 22. Garcia-Martinez L, Zhang Y, Nakata Y, et al. Epigenetic mechanisms in breast cancer
706 therapy and resistance. Nat Commun. 2021;12(1):1786.
707 23. Wong H, Leung R, Kwong A, et al. Integrating molecular mechanisms and clinical
708 evidence in the management of trastuzumab resistant or refractory HER-2(+) metastatic
709 breast cancer. Oncologist. 2011;16(11):1535-46.
710 24. Doench JG, Fusi N, Sullender M, et al. Optimized sgRNA design to maximize activity and
711 minimize off-target effects of CRISPR-Cas9. Nat Biotechnol. 2016;34(2):184-91.
712 25. Sanson KR, Hanna RE, Hegde M, et al. Optimized libraries for CRISPR-Cas9 genetic
713 screens with multiple modalities. Nat Commun. 2018;9(1):5416.
714 26. O'Geen H, Ren C, Nicolet CM, et al. dCas9-based epigenome editing suggests
715 acquisition of histone methylation is not sufficient for target gene repression. Nucleic Acids
716 Res. 2017;45(17):9901-16.
717 27. Ewald JD, Zhou G, Lu Y, et al. Web-based multi-omics integration using the Analyst
718 software suite. Nat Protoc. 2024.
719 28. Ramirez F, Ryan DP, Gruning B, et al. deepTools2: a next generation web server for
720 deep-sequencing data analysis. Nucleic Acids Res. 2016;44(W1):W160-5.
721 29. Krueger F, Andrews SR. Bismark: a flexible aligner and methylation caller for
722 Bisulfite-Seq applications. Bioinformatics. 2011;27(11):1571-2.
723 30. Clark AS, Yau C, Wolf DM, et al. Neoadjuvant T-DM1/pertuzumab and

724 paclitaxel/trastuzumab/pertuzumab for HER2(+) breast cancer in the adaptively randomized
725 I-SPY2 trial. Nat Commun. 2021;12(1):6428.
726 31. Dixon SJ, Olzmann JA. The cell biology of ferroptosis. Nat Rev Mol Cell Biol. 2024.
727 32. Ye L, Wen X, Qin J, et al. Metabolism-regulated ferroptosis in cancer progression and
728 therapy. Cell Death Dis. 2024;15(3):196.
729 33. Musolino A, Gradishar WJ, Rugo HS, et al. Role of Fcgamma receptors in HER2-targeted
730 breast cancer therapy. J Immunother Cancer. 2022;10(1).
731 34. Lee YS, Kalimuthu K, Park YS, et al. BAX-dependent mitochondrial pathway mediates the
732 crosstalk between ferroptosis and apoptosis. Apoptosis. 2020;25(9-10):625-31.
733 35. Jin ML, Jeong KW. Histone modifications in drug-resistant cancers: From a cancer stem
734 cell and immune evasion perspective. Exp Mol Med. 2023;55(7):1333-47.
735 36. Millan-Zambrano G, Burton A, Bannister AJ, et al. Histone post-translational modifications
736 - cause and consequence of genome function. Nat Rev Genet. 2022;23(9):563-80.
737 37. Piunti A, Shilatifard A. Epigenetic balance of gene expression by Polycomb and
738 COMPASS families. Science. 2016;352(6290):aad9780.
739 38. Mattei AL, Bailly N, Meissner A. DNA methylation: a historical perspective. Trends Genet.
740 2022;38(7):676-707.
741 39. Faubert B, Solmonson A, DeBerardinis RJ. Metabolic reprogramming and cancer
742 progression. Science. 2020;368(6487).
743 40. Kim J, DeBerardinis RJ. Mechanisms and Implications of Metabolic Heterogeneity in
744 Cancer. Cell Metab. 2019;30(3):434-46.
745 41. Stine ZE, Schug ZT, Salvino JM, et al. Targeting cancer metabolism in the era of

746 precision oncology. Nat Rev Drug Discov. 2022;21(2):141-62.

747 42. Bonifacio VDB, Pereira SA, Serpa J, et al. Cysteine metabolic circuitries: druggable

748 targets in cancer. Br J Cancer. 2021;124(5):862-79.

749 43. Koppula P, Zhuang L, Gan B. Cystine transporter SLC7A11/xCT in cancer: ferroptosis,

750 nutrient dependency, and cancer therapy. Protein Cell. 2021;12(8):599-620.

751 44. Lennicke C, Cocheme HM. Redox metabolism: ROS as specific molecular regulators of

752 cell signaling and function. Mol Cell. 2021;81(18):3691-707.

753 45. Sies H, Mailloux RJ, Jakob U. Fundamentals of redox regulation in biology. Nat Rev Mol

754 Cell Biol. 2024.

755 46. Wu K, El Zowalaty AE, Sayin VI, et al. The pleiotropic functions of reactive oxygen

756 species in cancer. Nat Cancer. 2024;5(3):384-99.

757 47. Stockwell BR. Ferroptosis turns 10: Emerging mechanisms, physiological functions, and

758 therapeutic applications. Cell. 2022;185(14):2401-21.

759 48. Dixon SJ, Lemberg KM, Lamprecht MR, et al. Ferroptosis: an iron-dependent form of

760 nonapoptotic cell death. Cell. 2012;149(5):1060-72.

761 49. Badgley MA, Kremer DM, Maurer HC, et al. Cysteine depletion induces pancreatic tumor

762 ferroptosis in mice. Science. 2020;368(6486):85-9.

763 50. Shi Z, Naowarojna N, Pan Z, et al. Multifaceted mechanisms mediating cystine

764 starvation-induced ferroptosis. Nat Commun. 2021;12(1):4792.

765 51. Yang F, Xiao Y, Ding JH, et al. Ferroptosis heterogeneity in triple-negative breast cancer

766 reveals an innovative immunotherapy combination strategy. Cell Metab. 2023;35(1):84-100

767 e8.

768 52. Zhang HF, Klein Geltink RI, Parker SJ, et al. Transsulfuration, minor player or crucial for
769 cysteine homeostasis in cancer. Trends Cell Biol. 2022;32(9):800-14.
770 53. Kang YP, Mockabee-Macias A, Jiang C, et al. Non-canonical Glutamate-Cysteine Ligase
771 Activity Protects against Ferroptosis. Cell Metab. 2021;33(1):174-89 e7.
772 54. Fox DB, Garcia NMG, McKinney BJ, et al. NRF2 activation promotes the recurrence of
773 dormant tumour cells through regulation of redox and nucleotide metabolism. Nat Metab.
774 2020;2(4):318-34.
775 55. Parida PK, Marquez-Palencia M, Nair V, et al. Metabolic diversity within breast cancer
776 brain-tropic cells determines metastatic fitness. Cell Metab. 2022;34(1):90-105 e7.
777 56. Pope LE, Dixon SJ. Regulation of ferroptosis by lipid metabolism. Trends Cell Biol.
778 2023;33(12):1077-87.
779 57. Duan N, Hua Y, Yan X, et al. Unveiling Alterations of Epigenetic Modifications and
780 Chromatin Architecture Leading to Lipid Metabolic Reprogramming during the Evolutionary
781 Trastuzumab Adaptation of HER2-Positive Breast Cancer. Adv Sci (Weinh). 2024:e2309424.
782 58. De Martino M, Rathmell JC, Galluzzi L, et al. Cancer cell metabolism and antitumour
783 immunity. Nat Rev Immunol. 2024.
784 59. Leone RD, Powell JD. Metabolism of immune cells in cancer. Nat Rev Cancer.
785 2020;20(9):516-31.
786 60. Chen X, Kang R, Kroemer G, et al. Broadening horizons: the role of ferroptosis in cancer.
787 Nat Rev Clin Oncol. 2021;18(5):280-96.
788 61. Cui JX, Xu XH, He T, et al. L-kynurenine induces NK cell loss in gastric cancer
789 microenvironment via promoting ferroptosis. J Exp Clin Cancer Res. 2023;42(1):52.

790 62. Poznanski SM, Singh K, Ritchie TM, et al. Metabolic flexibility determines human NK cell
791 functional fate in the tumor microenvironment. Cell Metab. 2021;33(6):1205-20 e5.
792 63. Han C, Ge M, Xing P, et al. Cystine deprivation triggers CD36-mediated ferroptosis and
793 dysfunction of tumor infiltrating CD8(+) T cells. Cell Death Dis. 2024;15(2):145.
794 64. Dang Q, Sun Z, Wang Y, et al. Ferroptosis: a double-edged sword mediating immune
795 tolerance of cancer. Cell Death Dis. 2022;13(11):925.
796 65. Zhou Q, Meng Y, Li D, et al. Ferroptosis in cancer: From molecular mechanisms to
797 therapeutic strategies. Signal Transduct Target Ther. 2024;9(1):55.
798 66. Boumahdi S, de Sauvage FJ. The great escape: tumour cell plasticity in resistance to
799 targeted therapy. Nat Rev Drug Discov. 2020;19(1):39-56.
800 67. Gatenby RA, Brown JS. Integrating evolutionary dynamics into cancer therapy. Nat Rev
801 Clin Oncol. 2020;17(11):675-86.
802 68. Polyak K. Breast cancer: origins and evolution. J Clin Invest. 2007;117(11):3155-63.
803 69. Chaffer CL, Weinberg RA. Cancer cell of origin: spotlight on luminal progenitors. Cell
804 Stem Cell. 2010;7(3):271-2.
805 70. Lim E, Vaillant F, Wu D, et al. Aberrant luminal progenitors as the candidate target
806 population for basal tumor development in BRCA1 mutation carriers. Nat Med.
807 2009;15(8):907-13.
808 71. Prat A, Perou CM. Mammary development meets cancer genomics. Nat Med.
809 2009;15(8):842-4.
810 72. Tharmapalan P, Mahendralingam M, Berman HK, et al. Mammary stem cells and
811 progenitors: targeting the roots of breast cancer for prevention. EMBO J.

812 2019;38(14):e100852.

813 73. Findlay GM, Daza RM, Martin B, et al. Accurate classification of BRCA1 variants with
814 saturation genome editing. Nature. 2018;562(7726):217-22.

815 74. Bailey SD, Desai K, Kron KJ, et al. Noncoding somatic and inherited single-nucleotide
816 variants converge to promote ESR1 expression in breast cancer. Nat Genet.
817 2016;48(10):1260-6.

818 75. Nishimura T, Kakiuchi N, Yoshida K, et al. Evolutionary histories of breast cancer and
819 related clones. Nature. 2023;620(7974):607-14.

820 76. Anandhan A, Dodson M, Schmidlin CJ, et al. Breakdown of an Ironclad Defense System:
821 The Critical Role of NRF2 in Mediating Ferroptosis. Cell Chem Biol. 2020;27(4):436-47.

822 77. Bai X, Ni J, Beretov J, et al. Activation of the eIF2alpha/ATF4 axis drives triple-negative
823 breast cancer radioresistance by promoting glutathione biosynthesis. Redox Biol.
824 2021;43:101993.

825 78. Wang Y, Hu J, Wu S, et al. Targeting epigenetic and posttranslational modifications
826 regulating ferroptosis for the treatment of diseases. Signal Transduct Target Ther.
827 2023;8(1):449.

828 79. Wang N, Ma T, Yu B. Targeting epigenetic regulators to overcome drug resistance in
829 cancers. Signal Transduct Target Ther. 2023;8(1):69.

830 80. Sun L, Zhang H, Gao P. Metabolic reprogramming and epigenetic modifications on the
831 path to cancer. Protein Cell. 2022;13(12):877-919.

832 81. Zhao S, Allis CD, Wang GG. The language of chromatin modification in human cancers.
833 Nat Rev Cancer. 2021;21(7):413-30.

834 82. Chen K, Chen Z, Wu D, et al. Broad H3K4me3 is associated with increased transcription
835 elongation and enhancer activity at tumor-suppressor genes. Nat Genet.
836 2015;47(10):1149-57.
837 83. Marsolier J, Prompsy P, Durand A, et al. H3K27me3 conditions chemotolerance in
838 triple-negative breast cancer. Nat Genet. 2022;54(4):459-68.
839 84. Duan N, Hua Y, Yan X, et al. An Imbalance in Histone Modifiers Induces tRNA-Cys-GCA
840 Overexpression and tRF-27 Accumulation by Attenuating Promoter H3K27me3 in Primary
841 Trastuzumab-Resistant Breast Cancer. Cancers (Basel). 2024;16(6).
842 85. Nishiyama A, Nakanishi M. Navigating the DNA methylation landscape of cancer. Trends
843 Genet. 2021;37(11):1012-27.
844 86. Sher G, Salman NA, Khan AQ, et al. Epigenetic and breast cancer therapy: Promising
845 diagnostic and therapeutic applications. Semin Cancer Biol. 2022;83:152-65.
846 87. Sukocheva OA, Lukina E, Friedemann M, et al. The crucial role of epigenetic regulation in
847 breast cancer anti-estrogen resistance: Current findings and future perspectives. Semin
848 Cancer Biol. 2022;82:35-59.
849 88. Palomeras S, Diaz-Lagares A, Vinas G, et al. Epigenetic silencing of TGFBI confers
850 resistance to trastuzumab in human breast cancer. Breast Cancer Res. 2019;21(1):79.
851 89. Jahangiri R, Jamialahmadi K, Gharib M, et al. Expression and clinicopathological
852 significance of DNA methyltransferase 1, 3A and 3B in tamoxifen-treated breast cancer
853 patients. Gene. 2019;685:24-31.
854 90. Du J, Johnson LM, Jacobsen SE, et al. DNA methylation pathways and their crosstalk
855 with histone methylation. Nat Rev Mol Cell Biol. 2015;16(9):519-32.

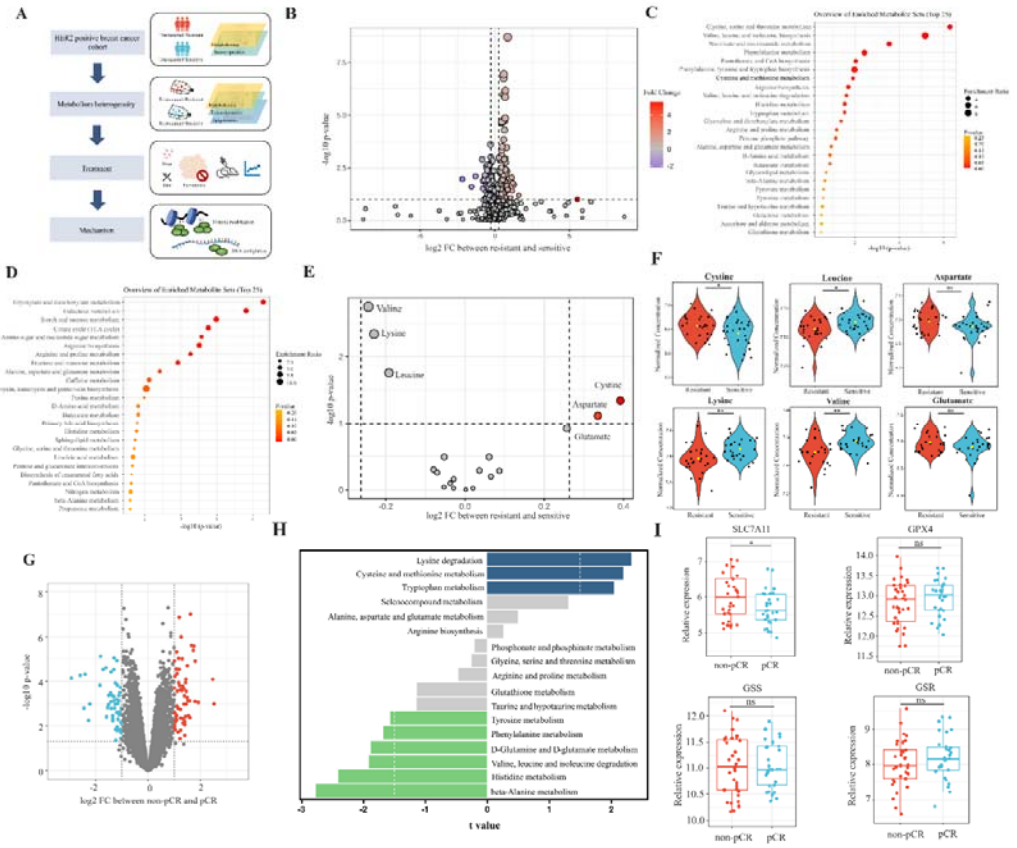

Figure 1. Analyses of amino acids metabolic patterns in trastuzumab primary resistant and sensitive HER2 positive breast cancer patients. (A) Workflow of analyses performed in this study. (B) Volcano plot of different circulating metabolites in the comparison between trastuzumab primary resistant and sensitive patients. (C) Enrichment analysis of circulating metabolites downregulated in trastuzumab primary resistant patients. (D) Enrichment analysis of circulating metabolites upregulated in trastuzumab primary resistant patients. (E-F) Volcano plot (E) and violin plots (F) of different circulating protein-construction amino acids in the comparison between trastuzumab primary resistant and sensitive patients. (G) Volcano plot of different genes between non-pCR and pCR patients in trastuzumab-based neoadjuvant treatment (I-SPY2, GSE181574). (H) Amino acids metabolic pathway analysis of non-pCR and pCR patients. (I) Relations between cysteine metabolic genes and trastuzumab treatment outcomes. Significances were determined by two-tailed unpaired t-test (F, I). ns, $P \geq 0.05$; *, $P < 0.05$; **, $P < 0.01$; ***, $P < 0.001$.

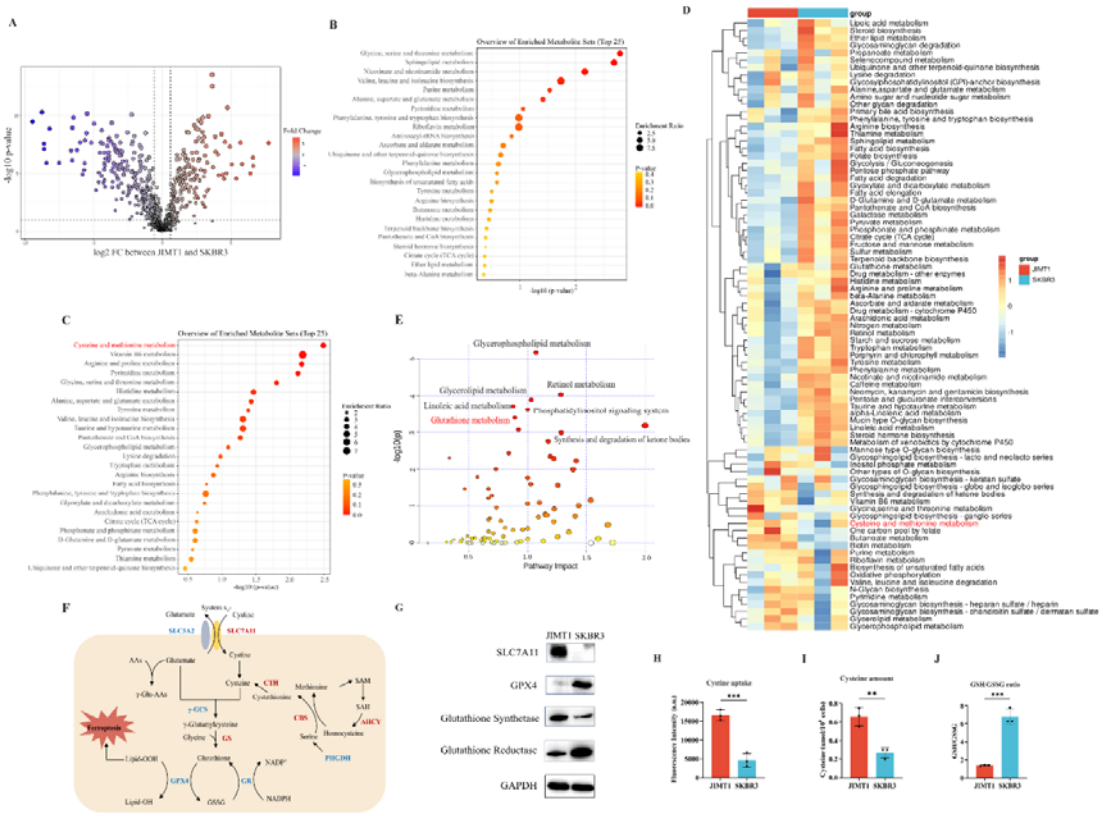

Figure 2. Heterogeneity of cysteine metabolism characteristics in HER2 positive breast cancer with different trastuzumab responses. (A) Volcano plot of hydrophilic metabolites in JIMT1 and SKBR3. (B) Upregulated metabolic processes in JIMT1 based on enrichment analysis of metabolites. (C) Downregulated metabolic processes in JIMT1 based on enrichment analysis of metabolites. (D) Different metabolic activities between JIMT1 and SKBR3 based on transcriptomics data. (E) Joint pathway analysis based on metabolomics and transcriptomics data. (F) Map of essential genes involved with cystine/cysteine metabolism. Upregulated genes in JIMT1 are highlighted in red and downregulated genes in JIMT1 are highlighted in blue. (G) Expression of essential proteins participating in cysteine and glutathione metabolism. (H) The comparison of cystine uptake ability between JIMT1 and SKBR3. (I) The comparison of intracellular cysteine abundance between JIMT1 and SKBR3. (J) The comparison of GSH:GSSG ratio between JIMT1 and SKBR3. Significances were determined by two-tailed unpaired t-test (H-J). ns, $P \geq 0.05$; *, $P < 0.05$; **, $P < 0.01$; ***, $P < 0.001$.

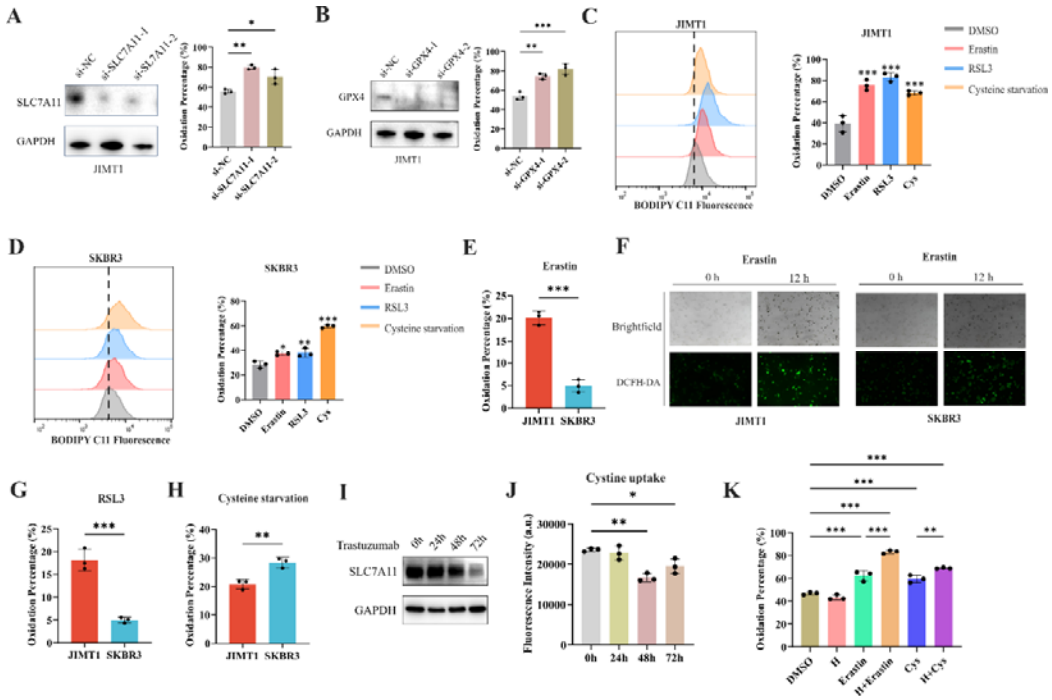

Figure 3. Ferroptosis sensitivity of HER2 positive breast cancer with different trastuzumab response. (A-B) Knockdown of SLC7A11 (A) and GPX4 (B) induced increased lipid peroxidation (BODIPY-C11) in JIMT1. (C-D) Treatment with erastin (10μm), RSL3 (1μm) and cysteine starvation for 12 hours induced lipid peroxidation (BODIPY-C11) in JIMT1 (C) and SKBR3 (D). (E-F) JIMT1 and SKBR3 featured different lipid peroxidation sensitivity to erastin by measuring BODIPY-C11 (E) and DCFH-DA (F). (G-H) JIMT1 and SKBR3 featured different lipid peroxidation sensitivity to RSL3 (G) and cysteine starvation (H). (I) SLC7A11 expression under different trastuzumab treatment time. (J) Cystine uptake ability under different trastuzumab treatment time. (K) The combination of erastin or cysteine starvation and trastuzumab increased lipid peroxidation in JIMT1. H, trastuzumab; Cys, cysteine starvation. Significances were determined by one-way ANOVA (A-D, J, K) and two-tailed unpaired t-test (E, G, H). ns, $P \geq 0.05$; *, $P < 0.05$; **, $P < 0.01$; ***, $P < 0.001$.

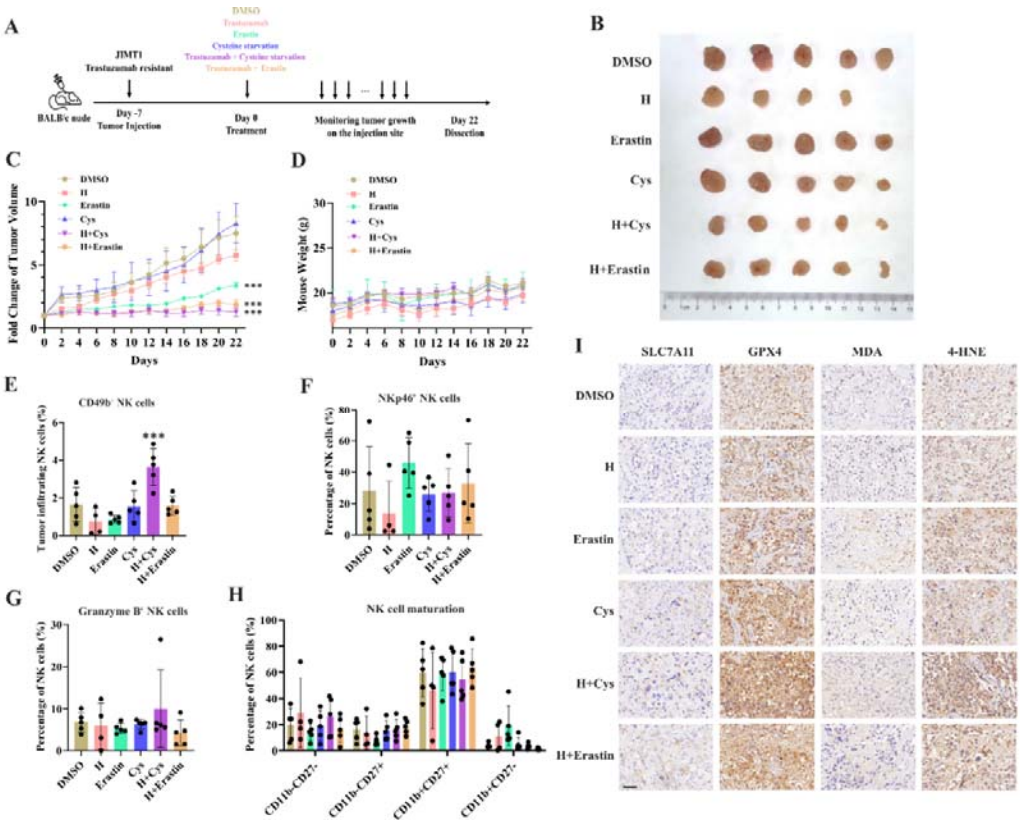

Figure 4. Targeting cysteine metabolism synergizes with trastuzumab to induce ferroptosis. (A) Schematic outline of treatment on cysteine metabolism in trastuzumab resistant breast cancer. JIMT1 cells were injected into the mammary fat pads of BALB/c nude mice at day -7. Treatment with DMSO, erastin, cysteine starvation, trastuzumab combined with or without erastin and cysteine starvation started at day 0 for 21 days. Tumor volume and mice weight were measured. The tumor growth was compared by paired individual fold change of tumor volumes. (B) Tumor of different treatment groups. (C) Fold change of tumor volume in different treatment groups. (D) Mice weight of different treatment groups. (E-H) Abundance of CD49b+ (E), NKp46+ (F), Granzyme B+ (G) and different development status (H) tumor infiltrating NK cells. (I) Representing immunohistochemistry images of SLC7A11, GPX4, MDA and 4-HNE in different treatment groups. Scale bar, 50 μm. H, trastuzumab; Cys, cysteine starvation. Significances were determined by two-way ANOVA (C, D) and one-way ANOVA (E-H). ns, $P \geq 0.05$; *, $P < 0.05$; **, $P < 0.01$; ***, $P < 0.001$.

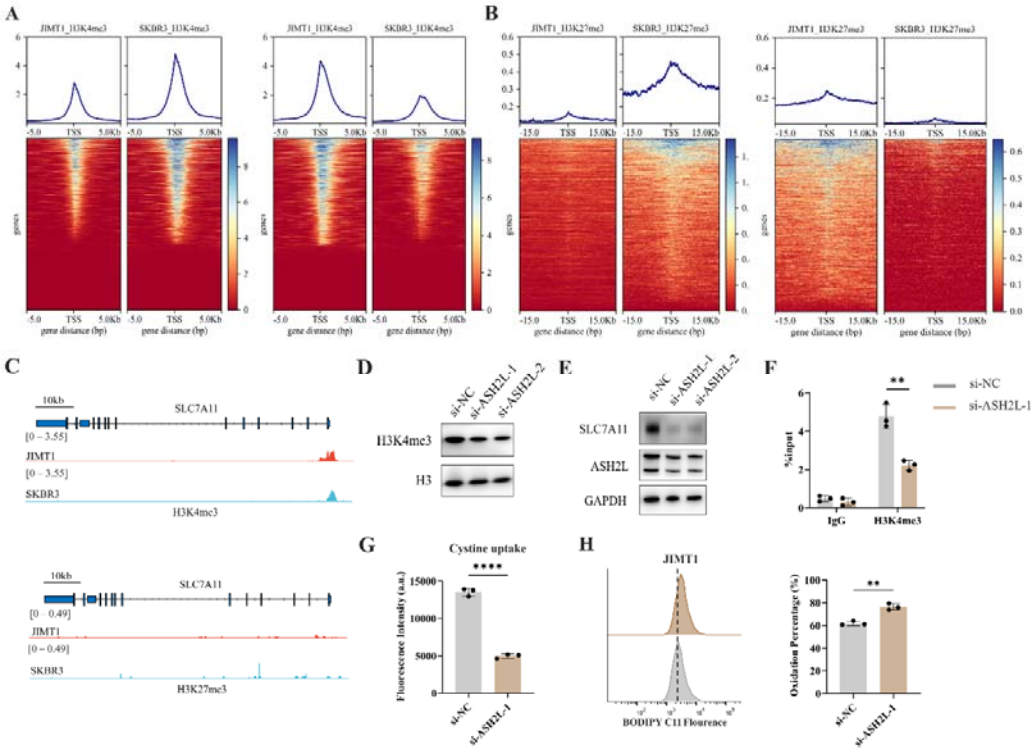

Figure 5. Increased H3K4me3 modifies SLC7A11 transcription and regulated cystine uptake. (A-B) Alterations of H3K4me3 (A) and H3K27me3 (B) peaks between JIMT1 and SKBR3. (C) Different abundance of H3K4me3 and H3K27me3 at SLC7A11 promoter regions in JIMT1 and SKBR3. (D) Decreased ASH2L inhibited total H3K4me3 expression. (E) Decreased ASH2L inhibited SLC7A11 expression. (F) Decreased ASH2L suppressed H3K4me3 expression at SLC7A11 promoter regions. (G) Decreased ASH2L suppressed cystine uptake ability. (H) Decreased ASH2L induced lipid peroxidation and ferroptosis. Significances were determined by two-tailed unpaired t-test (F-H). ns, $P \geq 0.05$; *, $P < 0.05$; **, $P < 0.01$; ***, $P < 0.001$.

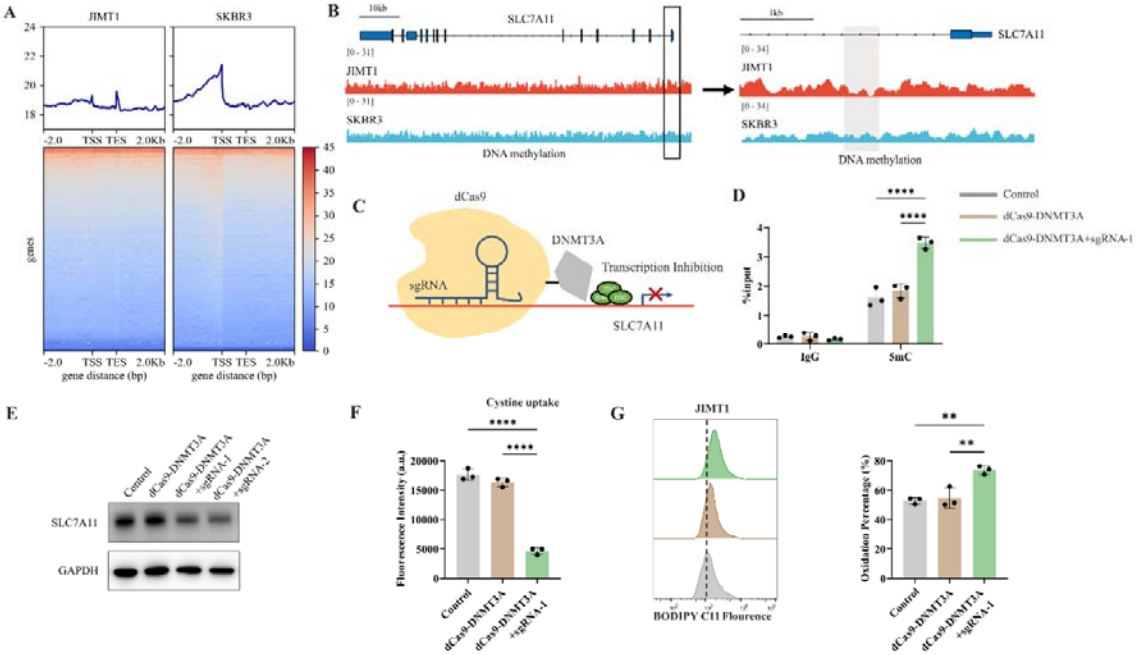

Figure 6. Decreased 5-mC modifications on SLC7A11 promoter relate with enhanced cystine uptake. (A) Alterations of 5-mC peaks between JIMT1 and SKBR3. (B) Different abundance of 5-mC at SLC7A11 promoter regions in JIMT1 and SKBR3. (C) Schematic outline of CRISPR-based epigenetic editing. dCas9-DNMT3A increased methylation of specific CpG islands in SLC7A11 promoter regions and inhibited gene transcription. (D) dCas9-DNMT3A increased 5-mC levels at SLC7A11 promoter regions. (E) dCas9-DNMT3A inhibited SLC7A11 expression. (F) dCas9-DNMT3A suppressed cystine uptake ability. (G) dCas9-DNMT3A induced lipid peroxidation and ferroptosis. Significances were determined by one-way ANOVA (D, F, G). ns, $P \geq 0.05$; *, $P < 0.05$; **, $P < 0.01$; ***, $P < 0.001$.

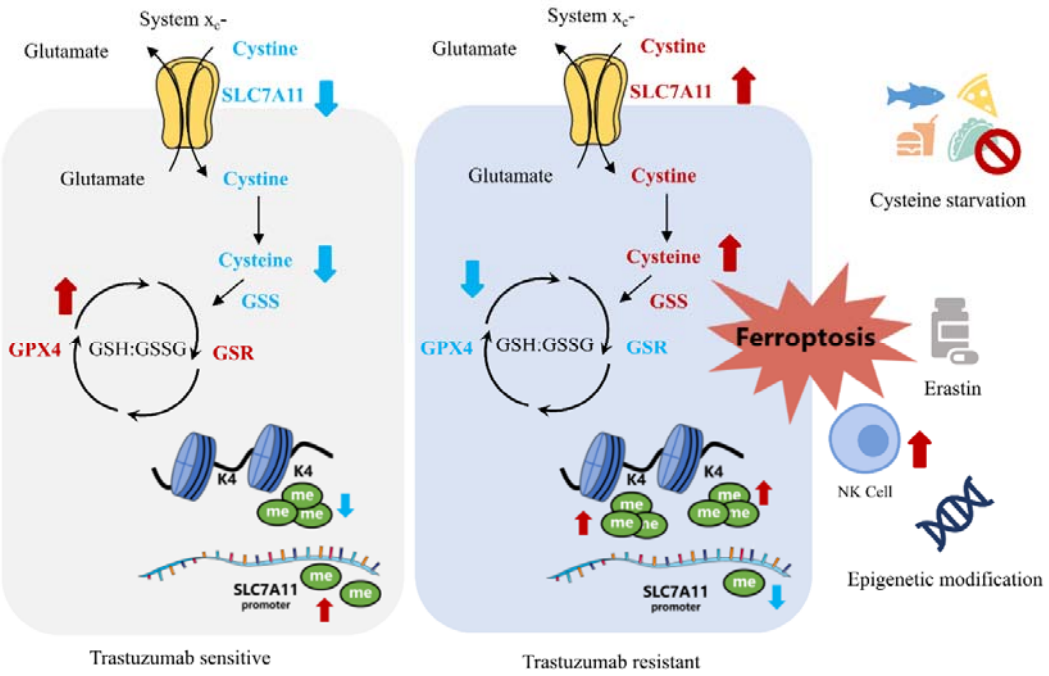

Figure 7. Summary of targeting cysteine metabolism in trastuzumab resistant HER2 positive breast cancer.

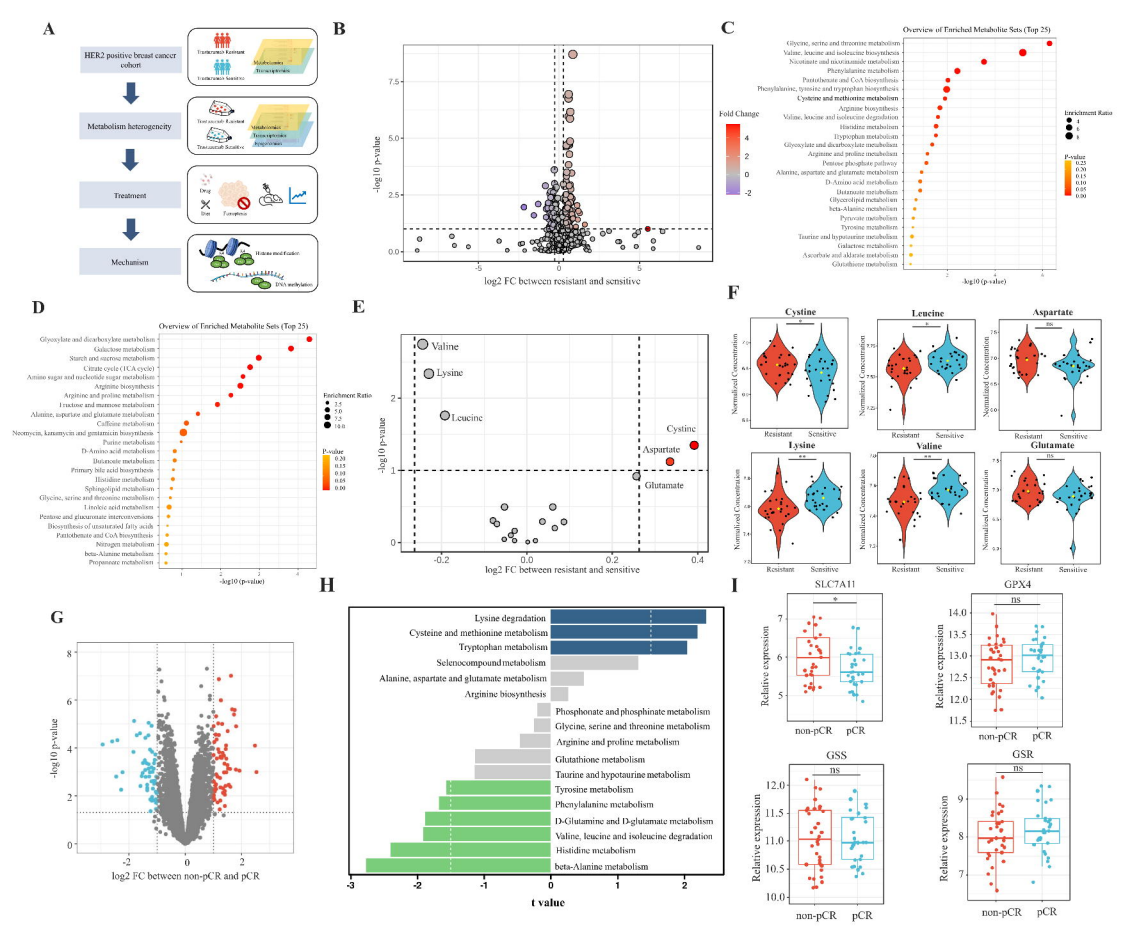
A
HER2 positive breast cancer cohort
Metabolism heterogeneity
Treatment
Mechanism
Trastuzumab Resistant
Trastuzumab Sensitive
Metabolomics
Transcriptomics
Drug
Stem
Ferroptosis
Histone modification
DNA methylation
B
-log10 p-value
log2 FC between resistant and sensitive
Fold Change
C
Overview of Enriched Metabolite Sets (Top 25)
Glycine, serine and threonine metabolism
Valine, leucine and isoleucine biosynthesis
Nicotinate and nicotinamide metabolism
Phenylalanine metabolism
Pantothenate and CoA biosynthesis
Phenylalanine, tyrosine and tryptophan biosynthesis
Cysteine and methionine metabolism
Arginine biosynthesis
Valine, leucine and isoleucine degradation
Histidine metabolism
Tryptophan metabolism
Glyoxylate and dicarboxylate metabolism
Arginine and proline metabolism
Pentose phosphate pathway
Alanine, aspartate and glutamate metabolism
D-Amino acid metabolism
Butanoate metabolism
Glycerolipid metabolism
beta-Alanine metabolism
Pyruvate metabolism
Tyrosine metabolism
Taurine and hypotaurine metabolism
Galactose metabolism
Ascorbate and aldarate metabolism
Glutathione metabolism
Enrichment Ratio
P-value
-log10 (p-value)
D
Overview of Enriched Metabolite Sets (Top 25)
Glyoxylate and dicarboxylate metabolism
Galactose metabolism
Starch and sucrose metabolism
Citrate cycle (TCA cycle)
Amino sugar and nucleotide sugar metabolism
Arginine biosynthesis
Arginine and proline metabolism
Fructose and mannose metabolism
Alanine, aspartate and glutamate metabolism
Caffeine metabolism
Neomycin, kanamycin and gentamicin biosynthesis
Purine metabolism
D-Amino acid metabolism
Butanoate metabolism
Primary bile acid biosynthesis
Histidine metabolism
Sphingolipid metabolism
Glycine, serine and threonine metabolism
Linoleic acid metabolism
Pentose and glucuronate interconversions
Biosynthesis of unsaturated fatty acids
Pantothenate and CoA biosynthesis
Nitrogen metabolism
beta-Alanine metabolism
Propanoate metabolism
Enrichment Ratio
P-value
-log10 (p-value)
E
Valine
Lysine
Leucine
Cystine
Aspartate
Glutamate
-log10 p-value
log2 FC between resistant and sensitive
F
Cystine
Leucine
Aspartate
Lysine
Valine
Glutamate
Normalized Concentration
Resistant
Sensitive
G
-log10 p-value
log2 FC between non-pCR and pCR
H
Lysine degradation
Cysteine and methionine metabolism
Tryptophan metabolism
Selenocompound metabolism
Alanine, aspartate and glutamate metabolism
Arginine biosynthesis
Phosphonate and phosphinate metabolism
Glycine, serine and threonine metabolism
Arginine and proline metabolism
Glutathione metabolism
Taurine and hypotaurine metabolism
Tyrosine metabolism
Phenylalanine metabolism
D-Glutamine and D-glutamate metabolism
Valine, leucine and isoleucine degradation
Histidine metabolism
beta-Alanine metabolism
t value
I
SLC7A11
GPX4
GSS
GSR
Relative expression
non-pCR
pCR

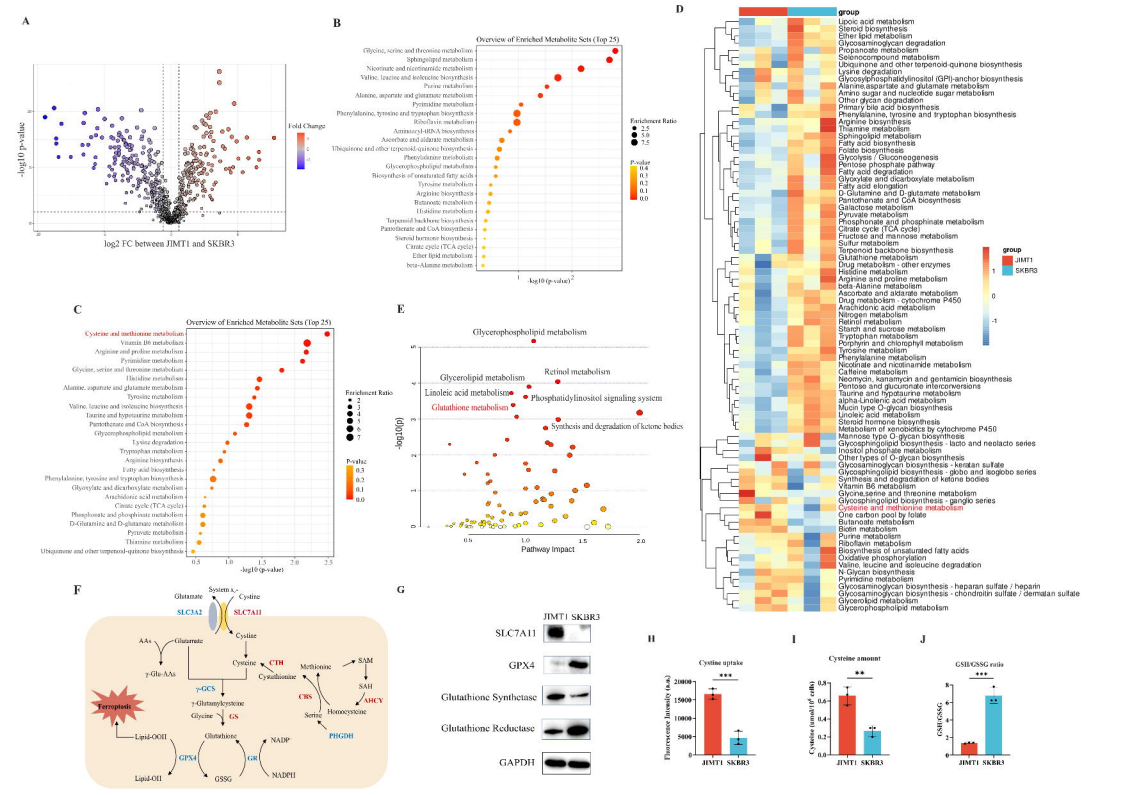
A
-log10 p-value
log2 FC between JIMT1 and SKBR3
Fold Change
B
Overview of Enriched Metabolite Sets (Top 25)
Glycine, serine and threonine metabolism
Sphingolipid metabolism
Nicotinate and nicotinamide metabolism
Valine, leucine and isoleucine biosynthesis
Purine metabolism
Alanine, aspartate and glutamate metabolism
Pyrimidine metabolism
Phenylalanine, tyrosine and tryptophan biosynthesis
Riboflavin metabolism
Aminoacyl-tRNA biosynthesis
Ascorbate and aldarate metabolism
Ubiquinone and other terpenoid-quinone biosynthesis
Phenylalanine metabolism
Glycerophospholipid metabolism
Biosynthesis of unsaturated fatty acids
Tyrosine metabolism
Arginine biosynthesis
Butanoate metabolism
Histidine metabolism
Terpenoid backbone biosynthesis
Pantothenate and CoA biosynthesis
Steroid hormone biosynthesis
Citrate cycle (TCA cycle)
Ether lipid metabolism
beta-Alanine metabolism
-log10 (p-value)
Enrichment Ratio
7.5
5.0
2.5
P-value
0.4
0.3
0.2
0.1
0.0
C
Overview of Enriched Metabolite Sets (Top 25)
Cysteine and methionine metabolism
Vitamin B6 metabolism
Arginine and proline metabolism
Pyrimidine metabolism
Glycine, serine and threonine metabolism
Histidine metabolism
Alanine, aspartate and glutamate metabolism
Tyrosine metabolism
Valine, leucine and isoleucine biosynthesis
Taurine and hypotaurine metabolism
Pantothenate and CoA biosynthesis
Glycerophospholipid metabolism
Lysine degradation
Tryptophan metabolism
Arginine biosynthesis
Fatty acid biosynthesis
Phenylalanine, tyrosine and tryptophan biosynthesis
Glycolysis/ and gluconeogenesis
Arachidonic acid metabolism
Citrate cycle (TCA cycle)
Phosphonate and phosphinate metabolism
D-Glutamine and D-glutamate metabolism
Pyruvate metabolism
Thiamine metabolism
Ubiquinone and other terpenoid-quinone biosynthesis
-log10 (p-value)
Enrichment Ratio
7
6
5
4
3
2
P-value
0.3
0.2
0.1
0.0
D
group
JIMT1
SKBR3
Lipoic acid metabolism
Steroid biosynthesis
Ether lipid metabolism
Glycosaminoglycan degradation
Propanoate metabolism
Selenocompound metabolism
Ubiquinone and other terpenoid-quinone biosynthesis
Lysine degradation
Glycosylphosphatidylinositol (GPI)-anchor biosynthesis
Alanine,aspartate and glutamate metabolism
Amino sugar and nucleotide sugar metabolism
Other glycan degradation
Primary bile acid biosynthesis
Phenylalanine, tyrosine and tryptophan biosynthesis
Arginine biosynthesis
Thiamine metabolism
Sphingolipid metabolism
Fatty acid biosynthesis
Folate biosynthesis
Glycolysis / Gluconeogenesis
Pentose phosphate pathway
Fatty acid degradation
Glyoxylate and dicarboxylate metabolism
Fatty acid elongation
D-Glutamine and D-glutamate metabolism
Pantothenate and CoA biosynthesis
Galactose metabolism
Pyruvate metabolism
Phosphonate and phosphinate metabolism
Citrate cycle (TCA cycle)
Fructose and mannose metabolism
Sulfur metabolism
Terpenoid backbone biosynthesis
Glutathione metabolism
Drug metabolism - other enzymes
Histidine metabolism
Arginine and proline metabolism
beta-Alanine metabolism
Ascorbate and aldarate metabolism
Drug metabolism - cytochrome P450
Arachidonic acid metabolism
Nitrogen metabolism
Retinol metabolism
Starch and sucrose metabolism
Tryptophan metabolism
Porphyrin and chlorophyll metabolism
Tyrosine metabolism
Phenylalanine metabolism
Nicotinate and nicotinamide metabolism
Caffeine metabolism
Neomycin, kanamycin and gentamicin biosynthesis
Pentose and glucuronate interconversions
Taurine and hypotaurine metabolism
alpha-Linolenic acid metabolism
Mucin type O-glycan biosynthesis
Linoleic acid metabolism
Steroid hormone biosynthesis
Metabolism of xenobiotics by cytochrome P450
Mannose type O-glycan biosynthesis
Glycosylpid biosynthesis - lacto and neolacto series
Inositol phosphate metabolism
Other types of O-glycan biosynthesis
Glycosaminoglycan biosynthesis - keratan sulfate
Glycosphingolipid biosynthesis - globo and isoglobo series
Synthesis and degradation of ketone bodies
Vitamin B6 metabolism
Glycine,serine and threonine metabolism
Glycosphingolipid biosynthesis - ganglio series
Cysteine and methionine metabolism
One carbon pool by folate
Butanoate metabolism
Biotin metabolism
Purine metabolism
Riboflavin metabolism
Biosynthesis of unsaturated fatty acids
Oxidative phosphorylation
Valine, leucine and isoleucine degradation
N-Glycan biosynthesis
Pyrimidine metabolism
Glycosaminoglycan biosynthesis - heparan sulfate / heparin
Glycosaminoglycan biosynthesis - chondroitin sulfate / dermatan sulfate
Glycerolipid metabolism
Glycerophospholipid metabolism
1
0
-1
E
Glycerophospholipid metabolism
Glycerolipid metabolism
Linoleic acid metabolism
Glutathione metabolism
Retinol metabolism
Phosphatidylinositol signaling system
Synthesis and degradation of ketone bodies
-log10(p)
Pathway Impact
F
Glutamate
System x-
Cystine
SLC3A2
SLC7A11
AAs
γ-Glu-AAs
γ-GCS
Cysteine
CTH
Cystathionine
Methionine
SAM
SAH
AHCY
Homocysteine
CBS
Serine
PHGDH
γ-Glutamylcysteine
Glycine
GS
Glutathione
NADP+
NADPH
GR
GSSG
GPX4
Lipid-OOH
Lipid-OH
Ferroptosis
G
JIMT1
SKBR3
SLC7A11
GPX4
Glutathione Synthetase
Glutathione Reductase
GAPDH
H
Cysteine uptake
Fluorescence Intensity (a.u.)
***
JIMT1
SKBR3
I
Cysteine amount
Cysteine (nmol/10⁶ cells)
**
JIMT1
SKBR3
J
GSH/GSSG ratio
GSH/GSSG
***
JIMT1
SKBR3

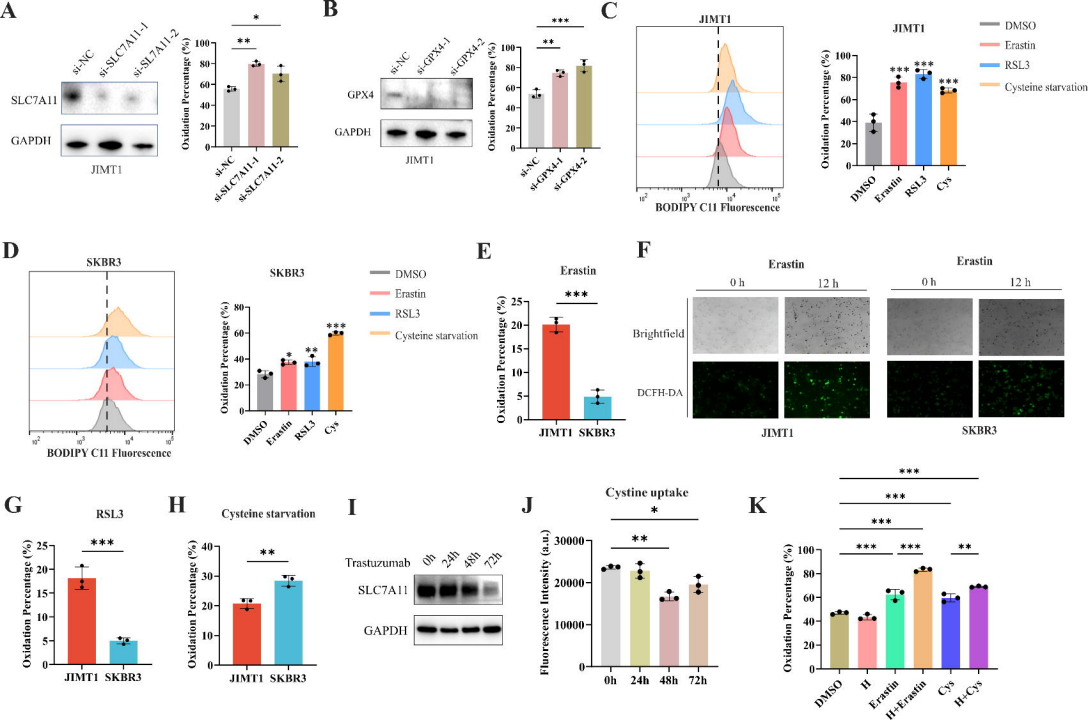
A
si-NC
si-SLC7A11-1
si-SLC7A11-2
SLC7A11
GAPDH
JIMT1
Oxidation Percentage (%)
B
si-NC
si-GPX4-1
si-GPX4-2
GPX4
GAPDH
JIMT1
Oxidation Percentage (%)
C
JIMT1
BODIPY C11 Fluorescence
DMSO
Erastin
RSL3
Cysteine starvation
Oxidation Percentage (%)
D
SKBR3
BODIPY C11 Fluorescence
DMSO
Erastin
RSL3
Cysteine starvation
Oxidation Percentage (%)
E
Erastin
Oxidation Percentage (%)
JIMT1
SKBR3
F
Erastin
0 h
12 h
Brightfield
DCFH-DA
JIMT1
SKBR3
G
RSL3
Oxidation Percentage (%)
JIMT1
SKBR3
H
Cysteine starvation
Oxidation Percentage (%)
JIMT1
SKBR3
I
Trastuzumab
0h
24h
48h
72h
SLC7A11
GAPDH
J
Cystine uptake
Fluorescence Intensity (a.u.)
0h
24h
48h
72h
K
Oxidation Percentage (%)
DMSO
H
Erastin
H+Erastin
Cys
H+Cys

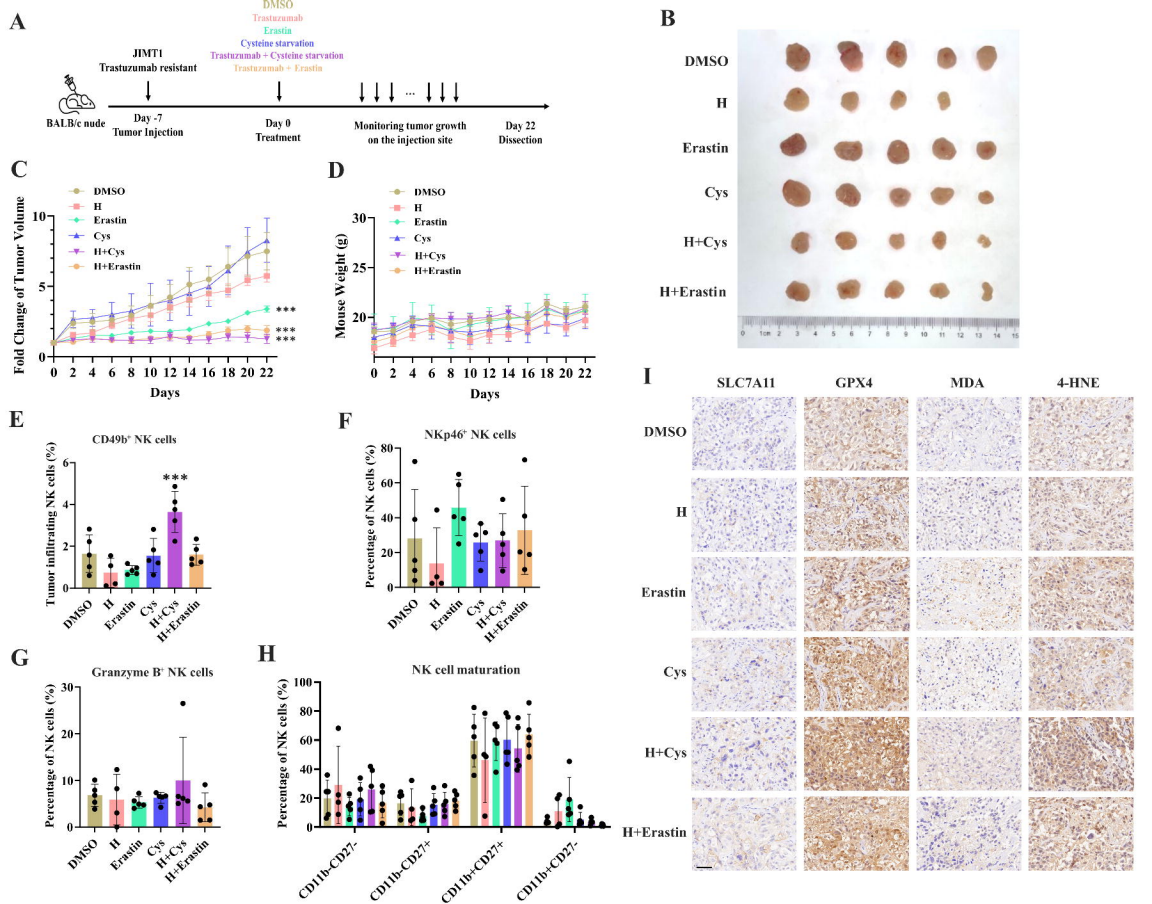
A
DMSO
Trastuzumab
Erastin
Cysteine starvation
Trastuzumab + Cysteine starvation
Trastuzumab + Erastin
JIMT1
Trastuzumab resistant
BALB/c nude
Day -7
Tumor Injection
Day 0
Treatment
Monitoring tumor growth
on the injection site
Day 22
Dissection
B
DMSO
H
Erastin
Cys
H+Cys
H+Erastin
C
Fold Change of Tumor Volume
Days
D
Mouse Weight (g)
Days
E
CD49b+ NK cells
Tumor infiltrating NK cells (%)
F
NKp46+ NK cells
Percentage of NK cells (%)
G
Granzyme B+ NK cells
Percentage of NK cells (%)
H
NK cell maturation
Percentage of NK cells (%)
CD11b-CD27-
CD11b-CD27+
CD11b+CD27+
CD11b+CD27-
I
SLC7A11
GPX4
MDA
4-HNE

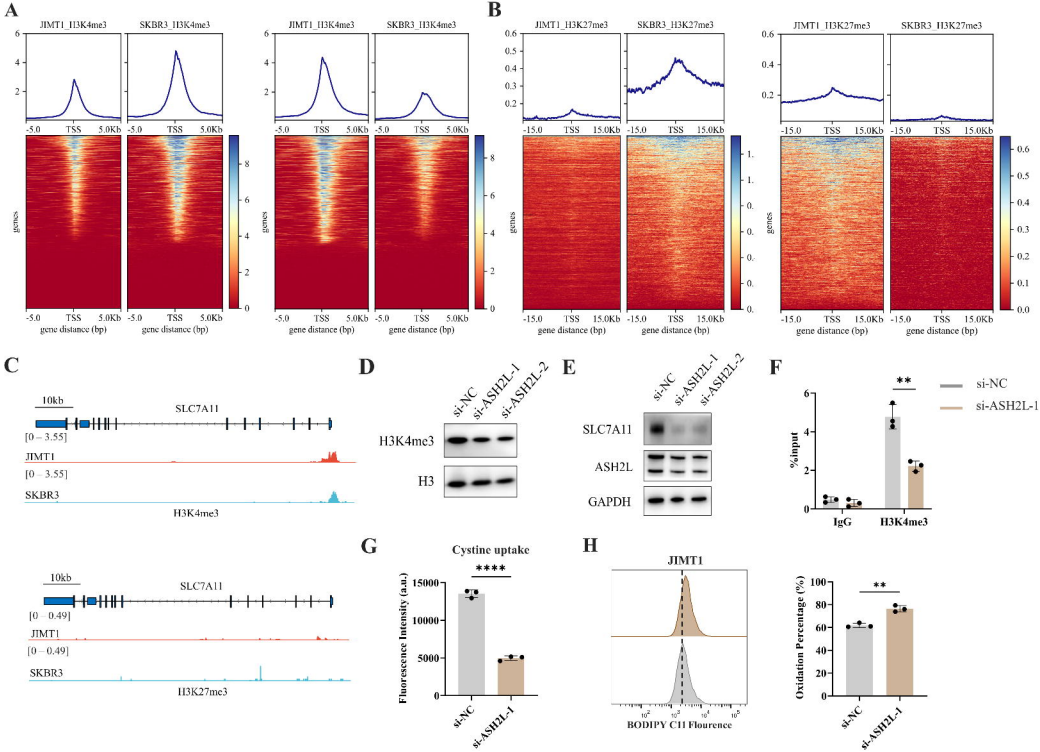
A
JIMT1_H3K4me3
SKBR3_H3K4me3
JIMT1_H3K4me3
SKBR3_H3K4me3
-5.0 TSS 5.0Kb
genes
gene distance (bp)
B
JIMT1_H3K27me3
SKBR3_H3K27me3
JIMT1_H3K27me3
SKBR3_H3K27me3
-15.0 TSS 15.0Kb
C
10kb
SLC7A11
[0 – 3.55]
JIMT1
SKBR3
H3K4me3
[0 – 0.49]
H3K27me3
D
si-NC
si-ASH2L-1
si-ASH2L-2
H3K4me3
H3
E
SLC7A11
ASH2L
GAPDH
F
si-NC
si-ASH2L-1
%input
IgG
H3K4me3
G
Cystine uptake
Fluorescence Intensity (a.u.)
H
JIMT1
BODIPY C11 Flourence
Oxidation Percentage (%)

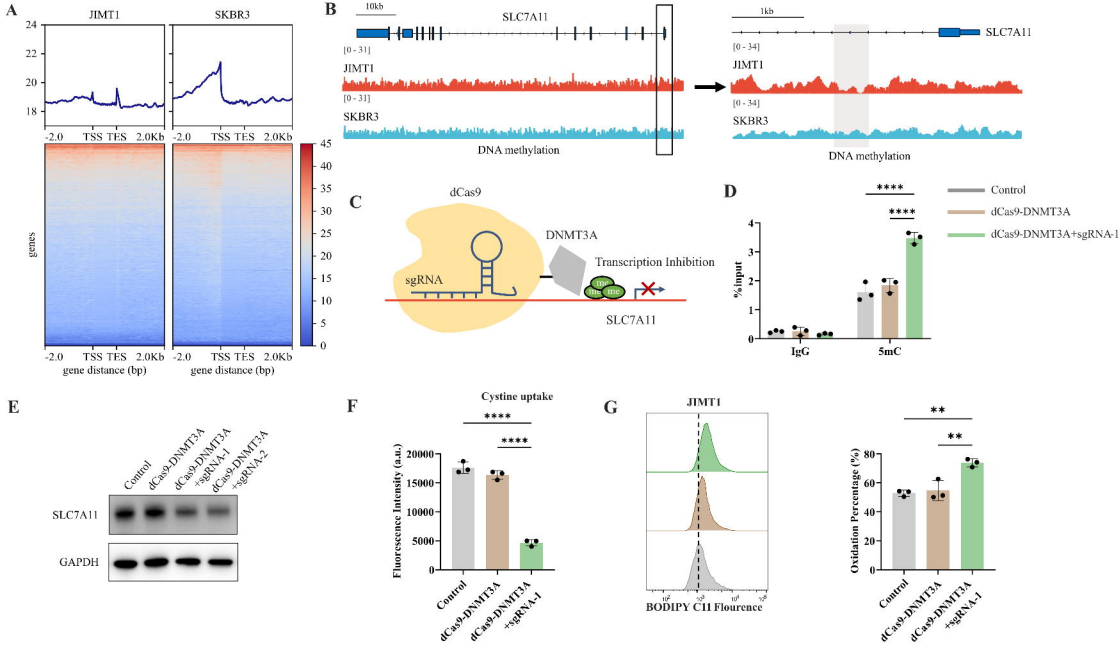
A
JIMT1
SKBR3
genes
-2.0 TSS TES 2.0Kb
gene distance (bp)
B
10kb
SLC7A11
[0 - 31]
JIMT1
SKBR3
DNA methylation
1kb
[0 - 34]
C
dCas9
DNMT3A
sgRNA
Transcription Inhibition
SLC7A11
D
Control
dCas9-DNMT3A
dCas9-DNMT3A+sgRNA-1
% Input
IgG
5mC
E
Control
dCas9-DNMT3A
dCas9-DNMT3A +sgRNA-1
dCas9-DNMT3A +sgRNA-2
SLC7A11
GAPDH
F
Cystine uptake
Fluorescence Intensity (a.u.)
G
JIMT1
BODIPY C11 Flourence
Oxidation Percentage (%)

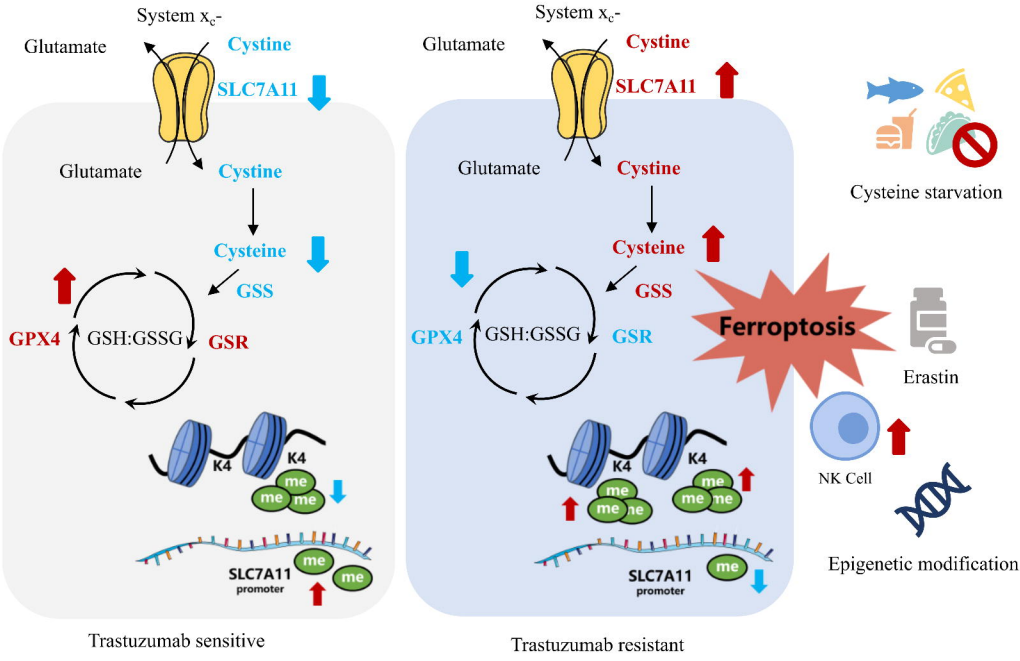
System x_c-
Glutamate
Cystine
SLC7A11
Glutamate
Cystine
Cysteine
GSS
GPX4
GSH:GSSG
GSR
K4
K4
me
me
me
me
me
me
SLC7A11
promoter
Trastuzumab sensitive
System x_c-
Glutamate
Cystine
SLC7A11
Glutamate
Cystine
Cysteine
GSS
GPX4
GSH:GSSG
GSR
K4
K4
me
me
me
me
me
me
me
SLC7A11
promoter
Trastuzumab resistant
Cysteine starvation
Ferroptosis
Erastin
NK Cell
Epigenetic modification